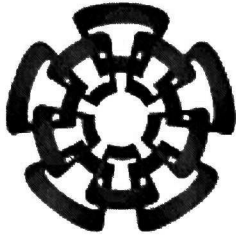


xx(92968.1)



CINVESTAV

Centro de Investigación y de Estudios Avanzados del IPN
Unidad Guadalajara

Modelos Avanzados para la Simulación de Transitorios Electromagnéticos en Líneas de Transmisión.

Tesis que presenta
Amner Israel Ramírez Vázquez

Para obtener el grado de
Doctor en Ciencias

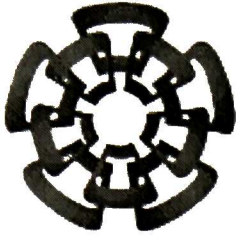
En la especialidad de
Ingeniería Eléctrica



CINVESTAV I.P.N.
SECCION DE INFORMACION
Y DOCUMENTACION

Guadalajara, Jal., Octubre del 2001

CLASIF.	Tesis 2002
ADQUIS.	
FECHA:	14/04/02
PROCED	Serv. Bibliotecarios



CINVESTAV

Centro de Investigación y de Estudios Avanzados del IPN
Unidad Guadalajara

Advanced Models for Electromagnetic Transient Simulation of Power Transmission Lines

Thesis submitted by
Amner Israel Ramírez Vázquez

For the degree of
Doctor of Sciences

In the specialty of
Electrical Engineering

Guadalajara, Jal., October 2001

Modelos Avanzados para la Simulación de Transitorios Electromagnéticos en Líneas de Transmisión

**Tesis de Doctorado en Ciencias
Ingeniería Eléctrica**

Por:

Amner Israel Ramírez Vázquez

Ingeniero Electricista
Universidad de Guanajuato 1991-1996

Maestro en Ciencias en Ingeniería Eléctrica
Universidad de Guadalajara 1996-1998

Becario del CONACYT, expediente no. **113684**

Directores de Tesis
Dr. José Luis Naredo Villagrán /
Dr. Pablo Moreno Villalobos /

Advanced Models for Electromagnetic Transient Simulation of Power Transmission Lines

**Tesis de Doctorado en Ciencias
Ingeniería Eléctrica**

Por:

Amner Israel Ramírez Vázquez

Ingeniero Electricista
Universidad de Guanajuato 1991-1996

Maestro en Ciencias en Ingeniería Eléctrica
Universidad de Guadalajara 1996-1998

Becario del CONACYT, expediente no. **113684**

Directores de Tesis
Dr. José Luis Naredo Villagrán
Dr. Pablo Moreno Villalobos

ACKNOWLEDGMENTS

Because of space, I cannot mention all the names. But, do not worry, I have in my mind those people who have made my life pleasant.

My best acknowledgments and gratefulness to God, my family, parents, brothers and sisters.

Specially thanks a lot to Dr. Naredo, Dr. Moreno, Dr. Semlyen, Dr. Iravani and all the professors who have helped me in this career.

Thanks to my friends at CINVESTAV and U. of T.

Dedicated to Dina, Abner Jahir and the next baby.

Abner

ACKNOWLEDGMENTS	iii
INDEX	iv
LIST OF FIGURES	vi
ABSTRACT	viii
RESUMEN	ix
I INTRODUCTION		
1.1	Electromagnetic transient analysis of power systems	1
1.2	Transmission line modeling for transient analysis	2
1.3	Issues requiring further development	6
1.4	Problem statement, methodology and scope	6
II SINGLE-PHASE LINES WITH FREQUENCY DEPENDENCE AND CORONA EFFECTS		
2.1	Introduction	8
2.2	Overview of the method of Characteristics	9
2.3	Single-phase Line with skin effect	11
	2.3.1 Transient resistance in frequency domain	11
	2.3.2 Transient resistance rational fitting	13
2.4	Numerical convolution	15
2.5	Single-phase lines with corona and skin effects	17
2.6	Remarks	22

III MULTICONDUCTOR LINEAR LINE MODELING IN TIME DOMAIN INCLUDING FREQUENCY DEPENDENCE EFFECT

3.1	Introduction	23
3.2	Telegrapher's equations for lines with frequency dependent parameters	...								24
3.3	Transmission line equations and Characteristics	25
3.4	Numerical solution of line equations	28
3.5	Application examples	30
3.6	Remarks	37

IV MODELING OF NON-UNIFORM TRANSMISSION LINES FOR TIME DOMAIN SIMULATION OF ELECTROMAGNETIC TRANSIENTS

4.1	Introduction	38
4.2	Terminal relations in frequency domain for NUL	39
4.3	Time domain model for NUL	42
4.4	Applications	43
4.5	Discussion of results	49
4.6	Remarks	50

V CONCLUSIONS

5.1	Summary of results	51
5.2	Recommendations for further developments	52

REFERENCES	54
-------------------	-----	-----	-----	-----	-----	-----	-----	-----	-----	-----------

APPENDIX A

Damping properties of backward Euler integration rule	59
--	-----	-----	-----	-----	-----	-----	-----	-----	-----	-----------

APPENDIX B

Resumen extendido	61
--------------------------	-----	-----	-----	-----	-----	-----	-----	-----	-----	-----------

APPENDIX C

List of publications	70
-----------------------------	-----	-----	-----	-----	-----	-----	-----	-----	-----	-----------

CHAPTER II

- 2.1 Discretization mesh.
- 2.2 Fitting of $H(s)$ for single-phase line example.
- 2.3 Resulting voltage waveforms along the single-phase line example.
- 2.4 a) Wagner's experiment waveforms, and b) Characteristics' simulation waveforms.
- 2.5 a) Gary's model simulation waveforms, and b) Characteristics' simulation waveforms.

CHAPTER III

- 3.1 Discretization mesh.
- 3.2 Configuration for illuminated transmission line.
- 3.3 Voltages induced at the ends of the central phase for illuminated distribution line
 - a) side A, b) side B.
- 3.4 Configuration for highly asymmetric overhead line.
- 3.5 Open circuit voltages at the receiving end for highly asymmetric overhead line
 - a) Conductor 1, b) Conductor 6, c) Conductor 9.
- 3.6 Configuration for underground cable system.
- 3.7 Open circuit voltages at the receiving end for underground cable system
 - a) core conductor 1, b) core conductor 3 and c) sheath conductor 6.

CHAPTER IV

- 4.1 Notation and reference directions for NUL.
- 4.2 Modal backward propagation functions for the three-phase symmetrical line of Fig. 4.6.
- 4.3 Modal backward propagation functions for the three-phase river crossing
 - a) $\rho_t = 10 \Omega\text{-m}$, b) $\rho_t = 1000\Omega\text{-m}$.
- 4.4 Modal backward propagation functions for the three-phase river crossing $\rho_t = 10 \Omega\text{-m}$.
- 4.5 Backward propagation function for the single-phase vertical structure.
- 4.6 Symmetrical, flat, three-phase NUL.
- 4.7 Time domain simulation and experimental results for the line of Fig. 4.6.
- 4.8 Simulations for the line of Fig. 4.6.
 - a) Characteristics, TD and NLT, b) NLT without considering non-uniform effects
- 4.9 Vertical structure.
- 4.10 Voltage at the top of vertical structure.
- 4.11 Current at the top of vertical structure.
- 4.12 Voltage at the bottom of vertical structure.
- 4.13 Profile of river crossing.
- 4.14 Voltage at the receiving end phases 1 and 3 for the line of Fig. 4.13.
- 4.15 Voltage at the receiving end phases 1 and 3 for the line of Fig. 4.13 using BE.

APPENDIX A

- A.1 Example for damping, time domain.

ABSTRACT

This thesis presents two methodologies for analyzing electromagnetic transients in multiconductor transmission systems. The first one is based on the method of Characteristics from the Partial Differential Equations Theory. The second one is based on state-space realizations and on traveling wave concepts.

Firstly, a Characteristics-based model for single-phase lines with frequency independent parameters and corona effect that was developed in [32], is extended here to include the frequency dependence of line parameters. This is achieved by taking as basis the Telegrapher's equations modified by Radulet, *et. al.* [11], which include the frequency dependence by means of a convolution term. Recursive convolutions are combined with Characteristics to incorporate this term into the new model. The results obtained with it agree well with experimental results.

Secondly, the Characteristics model with frequency dependence and without corona is extended to multiconductor line (cable) cases. This extension permits accounting for distributed sources, like those produced by radiated electromagnetic (EM) fields. It is shown that in these cases, the new model is more convenient and accurate than conventional representations based on EMTP [34]. The extended model can as well be applied to long homogeneous lines excited by lumped sources. In these cases it is computationally less efficient than recent traveling wave based models [39, 41, 44, 45]. Nevertheless, its pre-processing is much simpler and its simulation results are remarkably close to the ones obtained through the Numerical Laplace Transform (NLT) method.

Finally, the problem of producing time domain models for non-uniform multiconductor lines is approached. Such a model is attained by adopting a frequency domain methodology proposed in [38] and by applying state-space realization methods and recursive convolutions. The resulting model is benchmarked against NLT and field tests.

RESUMEN

Esta tesis presenta dos metodologías para analizar transitorios electromagnéticos en sistemas de transmisión multiconductores. El primero está basado en el método de las Características de la Teoría de Ecuaciones Diferenciales Parciales. El segundo está basado en realizaciones de espacio-estado y conceptos de ondas viajeras.

Primeramente, un modelo basado en Características para línea monofásica con parámetros independientes de la frecuencia y efecto corona que fue desarrollado en [32], es extendido aquí para incluir la dependencia frecuencial de los parámetros de línea. Esto es logrado tomando como base las ecuaciones del Telegrafista modificadas por Radulet, *et. al.* [11], el cual incluye la dependencia frecuencial por medio de un término de convolución. Convoluciones recursivas son combinadas con Características para incorporar este término dentro del nuevo modelo. Los resultados obtenidos con esto concuerdan bien con resultados experimentales.

Después, el modelo de Características con dependencia frecuencial y sin corona es extendido al caso multiconductor de líneas (cables). Esta extensión permite incluir fuentes distribuidas, como las producidas por campos electromagnéticos (EM) radiados. Se muestra que en estos casos, el nuevo modelo es más conveniente y exacto que representaciones convencionales basadas en EMTP [34]. El modelo extendido puede también ser aplicado a líneas homogéneas largas excitadas por fuentes concentradas. En estos casos es computacionalmente menos eficiente que recientes modelos basados en ondas viajeras [39, 41, 44, 45]. Sin embargo, su pre-procesamiento es mucho más simple y los resultados de su simulación son remarcablemente cercanos a los obtenidos a través del método de la Transformada Numérica de Laplace (TNL).

Finalmente, el problema de producir modelos en el dominio del tiempo para líneas multiconductoras no-uniformes es abordado. Tal modelo es obtenido adoptando una metodología en el dominio de la frecuencia propuesta en [38] y aplicando métodos de realizaciones de espacio-estado y convoluciones recursivas. El modelo resultante se compara con la TNL y pruebas de campo.

1.1 Electromagnetic transient analysis of power systems

The reliability of electric power systems depends, to a large extent, on an accurate design of transmission system elements such as overhead lines, underground cables, protections, etc. An important issue of system design is the analysis of electromagnetic transient performance. Traditionally, transient analysis was developed having in mind basically the problems of insulation design and of establishing withstand parameters. As the transient analysis become more accurate, it is possible to design less expensive and more reliable power systems. The costs of over-insulation of power systems often are very considerable. Apart from the insulation design problem, recently power system specialists have realized the importance of transient analysis tools in the testing of protection , control and measurement equipment.

The transient response of an electric system can be determined in principle from the system itself. This approach, however, has severe drawbacks. Firstly, it is very expensive to take out of service one of such systems. Secondly, for technical and economic reasons, transient excitations would have to be scaled down; but, since there are many non-linear effects, the system's response obtained may not be representative of full scale phenomena. Thirdly, there are multiple examples of perturbations that are neither reproducible nor controllable with experimental setups; for example, lightning stroke occurrences. Because of these limitations, mathematical modeling of power systems has been gaining importance to its actual status as an essential complement to physical tests.

Calculated transient waveforms have been used for sometime to do off-line tests of electronic instruments. Recently, electronic devices reproducing these calculated transients in real time are being employed by equipment manufacturers and by power utilities to do open-loop on line

testing. A very active area of research at present time is the development of digital real time simulators that are capable of testing electronic equipment in a closed-loop fashion.

1.2 Transmission line modeling for transient analysis

Transmission lines (and cables) are important constituents of power systems. The importance of their modeling for transient studies stems from the fact that lines often are taken as modeling elements. Early line models were based on the lossless case, for which the line equations are just a form of the Wave Equation. D'Alembert solution to the latter, in terms of traveling waves, is well known and is the basis for the well known model by Bergeron and for its circuitual representation by two Norton equivalents [19]. A considerable amount of effort has been placed for the last 30 years to extend this basic model to the lossy multiconductor line case.

Two of the first works on single-phase lines that considered the frequency dependence of the line parameters are by Budner in 1970 [7] and by Snelson in 1972 [8]. Their models are based on the relation of voltages and currents at the two ends of the line; *i. e.*, a two-port network in the frequency domain. The two-port parameters relating input/output voltages and currents are functions of frequency and usually are referred to as weighting functions (WFs). Due to the symmetry of the problem, when using the nodal representation only two of the four functions are different. These functions are highly oscillatory in the frequency domain and their proper representation in the time domain requires a large number of samples. In addition, the WFs time domain images present a large number of spikes and must be truncated, in order to perform numeric convolution processes. The solution of the propagation line equations was carried out by the above mentioned authors in time domain using long convolutions between the WFs and the corresponding voltages and currents.

For the passing from the single-phase to the multiconductor line case there are two possible approaches. One is called "The Phase Domain" and consists in dealing with electromagnetic couplings among the line conductors. The other is "The Modal Domain" which consists in obtaining n -decoupled systems equivalent to a single system of n -coupled conductors. This decoupling is attained by means of two modal transformation matrices which can be placed into a mutually orthogonal relationship [4].

In 1975 Semlyen and Dabuleanu proposed a method to solve convolutions in a recursive manner [10]. This method is applicable when one of the convolving functions is an exponential. Recursive convolution decreases computation time substantially. In their work, Semlyen and Dabuleanu applied recursive convolution and modal techniques to multiconductor transmission lines by considering real and constant modal transformation matrices.

In 1982 J. Martí proposed a model in which the terminals of the line are considered connected to a network that represents the characteristic impedance of the line for an entire range of frequencies [13]. Now, one of the WFs is zero and the other presents an initial spike only, thus reducing considerably the calculations required for the convolution. The characteristic impedance and the propagation function were synthesized by rational functions whose poles and zeros were obtained from a technique based on the graphical method by Bode. Martí's original model considered real and constant transformation matrices. In the cases of asymmetric, unbalanced or multicircuit transmission systems, however, the transformation matrices are highly dependent of frequency. This dependence should be taken into account if more accurate results are desired.

In 1988 L. Martí proposed a technique to take into account the frequency dependence of the transformation matrices [21]. In addition to the characteristic admittance and the propagation function, the transformation matrices must be synthesized by rational functions. This method was implemented for underground cables and, apparently, its extension to overhead lines had not been possible.

Gustavsen and Semlyen [44] in 1997 proposed a hybrid model that separated the propagation matrix in two parts to obtain smooth functions in the frequency. Additionally, these authors applied a technique called Vector Fitting (VF) in which all the elements of each column of the matrix are adjusted using the same poles. This reduced the number of calculations in the numerical evaluation of convolutions.

In 1997 Castellanos and J. Martí proposed a model in the phase domain denominated Z-Line [41]. In this model the line is formed of ideal line segments and losses and frequency dependent blocks are inserted between these segments. The frequency dependent part is synthesized with rational functions. In this work, an open issue is that of determining the optimum number of segments in

which a line is to be subdivided. In addition, these authors reported the appearance of numerical oscillations due to line subdivision.

A proposal to develop a line model in the phase domain was made by Nguyen, *et. al.*, in 1997 [42]. In this model, the characteristic admittance and the propagation function matrices are synthesized in the phase domain. The problem here was that the elements of these matrices are highly oscillatory functions. This was solved by multiplying by -1 all the non-diagonal elements and, in addition, a single delay factor was extracted from all the elements in the propagation matrix.

Based on an idempotent decomposition technique proposed by Wedepohl [15], J. Martí and Castellanos proposed in 1995 a method in which all the modal delays could be decoupled and extracted from a line's propagation matrix [35]. In 1997 Marcano and J. Martí fully developed the idempotent model [39,43]. In 1999 Morched, *et. al.*, combined the idempotent delay decoupling technique with VF into what is called nowadays as "The Universal Line Model" [45].

The universal or idempotent line model practically solves the problem of modeling in the time domain multiconductor lines that are homogeneous, linear and excited by lumped sources. Another important phenomenon, however, that some researchers have introduced in their line models is the "Corona Effect" In many cases, corona can produce more distortion on propagating waves of voltage and current than the one due to linear dispersion or "Skin Effect" The variation of the line capacitance with respect to the line voltage, and even to its rate of change, results in a mathematical non-linear problem.

In 1955 Wagner and Lloyd carried out, using the first digital computers available, a study of corona effect in the propagation of waves in single-phase lines [2]. Finite differences were used to integrate the Telegrapher's equations. Stafford, *et. al.*, in 1965 also proposed a program of the same type [6]. In the results of these two works the problem of numerical oscillations caused by the spatial discretization of the line equations was apparent. In 1983 Gary, *et. al.*, adopted the Telegrapher's equations for single-phase lines as modified by Radulet, *et. al.* These authors added to these equations the non-linearity caused by corona. They solved the Telegrapher's modified equations in the time domain through conventional finite difference methods and long convolutions. The resulting line model required excessive computational resources [16]. In 1986

Semlyen and Wei-Gang proposed a multiconductor line model with corona effect using state-variable techniques along with Bergeron's method [18]. In this model, conventional modal analysis was used. This, however, is appropriate only for linear system analysis.

Carneiro, *et. al.*, developed a model of lines with corona that was based on Bergeron's method [25,29]. In their work, the problem of numerical oscillations caused by the spatial discretization of the line was documented thoroughly. Noda and Ametani proposed in 1996 a model based on digital signal processing techniques that allows variable time steps. In this model, corona branches are introduced between sections of frequency dependent transmission lines. The problem of numerical oscillations appears also in this model [36]. In 1995 Naredo [32] introduced a finite difference method based on the Theory of Characteristics of Partial Differential Equations (PDEs) [9]. This model was applied successfully to single-phase lines with corona effect and without linear dispersion. It eliminated the numerical oscillations problem which appears even in recent models [48]. In addition, it was shown that the model is able to deal properly with multiple wave reflections in transmission lines [33]. The method of Characteristics appears, at present, as very promising for handling non-linear and non-uniform line problems.

In most transient analysis studies, lines are assumed as uniform and discontinuities are considered lumped. Recent experimental and simulation results show, however, that non-uniformities can be important. Examples of non-uniform lines (NULs) are: overhead lines with sagging conductors, lines entering substations, lines crossing rivers and vertical conductors. Several approaches have been proposed recently for handling NULs. Menemenlis and Chun in 1982 proposed one based on traveling waves and Bewley's Lattice Diagram for single-phase lossless line [14]. There are also two models of single-phase lines in which parameter variations are approximated by exponentials in a piecewise manner. One was proposed in 1994 by Oufi, *et. al.*, and was developed in the frequency domain [30]. The other was proposed in 1997, by Nguyen, *et. al.*, and was in the time domain [40]. A non-uniform model was proposed by Ishii, *et. al.*, in 1991 and applied to transmission towers. In this model, each section of the tower is represented by a frequency dependent line followed by a constant resistance shunted with a constant inductance [26]. The problem of this model is that some of the parameters must be taken from measurements.

Alternative models based on finite difference methods are used to solve the partial differential equations of the non-uniform line disregarding the frequency dependence of the parameters. One of these models was described in 1999 by Gutierrez, *et. al.*, in which the method of Characteristics was used [46]. The other model, which is based on discretizing directly the line equations by finite differences, was proposed in 1996 by Correia de Barros and Almeida [38]. Mamis and Koksai in 2001 described a single-phase model in the frequency domain that represents the transmission line as a two-port network, whose transfer matrix is obtained from the multiplication of the chain matrices of the lines sub-segments [49].

1.3 Issues requiring further development

Time domain line models based on traveling wave concepts can be considered at present well-established and permit simulating line sections that are homogeneous, linear and excited by lumped sources. There are many cases in practice, however, that require line subdivision; examples are: non-uniform lines [38,46], lines affected by corona (non-linear propagation) [2,23], lines affected by radiated fields [48] and uniform lines with multiple transpositions.

Most models being proposed for line subdivision are prone to numeric oscillations. The method of Characteristics solves this problem. It has been applied to single-phase lines with corona, but still has to be extended to include frequency dependence and multiconductor effects.

As for multiconductor NULs, there are two approaches that seem very promising. One is based on Characteristics and the other is based on synthesizing two-port relationships in the frequency domain and on applying recursive convolutions to produce a time domain model.

1.4 Problem statement, methodology and scope

A methodology is required for producing time domain models of lines that are affected by corona and linear dispersion and that are free of numeric oscillations, at least for the single-phase case. Also, a methodology to produce time domain models of multiconductor lines that are excited by distributed sources is required. Finally, a methodology for producing time domain models of NULs including frequency dependent and multiconductor effects is highly desirable.

In this thesis, the method of Characteristics of PDEs Theory is adopted first to produce a time domain model for single-phase lines affected by corona and by linear dispersion. Then, this model is extended and adapted for dealing with uniform lines that are multiconductor and frequency dependent when the excitation is by a distributed source. It is shown that this extended model handles highly asymmetric overhead lines and underground cables at least as effectively as the idempotent/universal line model. Finally, the problem of lines that are non-uniform, multiconductor and frequency dependent is approached employing the methodology of frequency domain synthesis and recursive convolutions for producing a time domain model.

II SINGLE-PHASE LINES WITH FREQUENCY DEPENDENCE AND CORONA EFFECTS

2.1 Introduction

Frequency variations of line parameters provoke progressive distortion and attenuation of transient waves during their propagation along transmission lines. This phenomenon is known as linear dispersion or skin effect. If only this effect is considered, a very accurate calculation of wave shapes can be obtained using frequency domain methods such as Fourier and Laplace transforms. On the other hand, when high voltage levels are considered, the occurrence of corona discharge produces changes in the instantaneous values of the line capacitance and conductance parameters. When corona takes place, the line capacitances become functions of voltage and this introduces non-linear features in the propagation phenomenon. Therefore, for solving accurately this non-linearity, time domain methods are preferable. A problem often encountered in the numerical solution of the non-linear PDEs representing a line is the appearance of numerical oscillations due to discretizations [2, 6, 18, 25, 29, 36, 48]. This numerical problem has been solved in [32] with the method of Characteristics from the PDE Theory [9]. Further advantages of this method are that it allows using large integration steps and that it can be extended to the multiconductor line case without resorting to conventional linear modal analysis.

In this chapter the method of Characteristics, based on a line model proposed by Radulet, *et. al.* [11], is combined with a technique proposed here for synthesizing line transient parameters. This permits solving the complete problem of electromagnetic transients in single-phase overhead lines considering both, linear dispersion and corona effect.

2.2 Overview of the method of Characteristics

For a line whose parameters are considered independent of frequency, the Telegrapher's equations can be represented as follows using matrix notation [32]:

$$\frac{\partial}{\partial t} \mathbf{u} + \mathbf{A} \frac{\partial}{\partial x} \mathbf{u} + \mathbf{B} \mathbf{u} = \mathbf{0}, \quad (2.1)$$

where, for an overhead single-phase line:

$$\mathbf{u} = \begin{bmatrix} v \\ i \end{bmatrix} \quad \mathbf{A} = \begin{bmatrix} 0 & 1/C \\ 1/L & 0 \end{bmatrix} \quad \text{and} \quad \mathbf{B} = \begin{bmatrix} 0 & 0 \\ 0 & R/L \end{bmatrix} \quad (2.2)$$

In (2.2) $v = v(x,t)$ and $i = i(x,t)$ are the line voltage and current, respectively; L , C and R are the inductance, capacitance and resistance line parameters in per unit length (p.u.l.), respectively.

The eigenvalues of \mathbf{A} are:

$$\lambda_{1,2} = \pm \frac{1}{\sqrt{LC}}. \quad (2.3a, b)$$

where the plus sign for λ_1 corresponds to the velocity of a wave traveling in the forward direction and the minus sign for λ_2 to a backward wave velocity. These eigenvalues are real and distinct implying that system (2.1) is hyperbolic [9]. A left eigenvector matrix for \mathbf{A} is as follows:

$$\mathbf{E}_{left} = \begin{bmatrix} 1 & Z_w \\ 1 & -Z_w \end{bmatrix}, \quad (2.4)$$

where $Z_w = \sqrt{L/C}$ is denominated the "wave impedance" [32]. Pre-multiplication of system (2.1) by matrix \mathbf{E}_{left} , followed by further algebraic manipulations, yields:

$$\left(\frac{\partial}{\partial t} + \lambda_1 \frac{\partial}{\partial x} \right) v + Z_w \left(\frac{\partial}{\partial t} + \lambda_1 \frac{\partial}{\partial x} \right) i + \lambda_1 R i = 0 \quad (2.5a)$$

and

$$\left(\frac{\partial}{\partial t} + \lambda_2 \frac{\partial}{\partial x} \right) v - Z_w \left(\frac{\partial}{\partial t} + \lambda_2 \frac{\partial}{\partial x} \right) i + \lambda_2 R i = 0 \quad (2.5b)$$

If (2.5a) and (2.5b) are restricted to the following curves referred to as "characteristics":

$$\frac{dx}{dt} = \pm \frac{1}{\sqrt{LC}}. \quad (2.6a, b)$$

the terms inside parenthesis in (2.5a) and (2.5b) represent total derivatives; hence (2.5a) and (2.5b) become the following ordinary differential equations:

$$dv + Z_w di + R i dx = 0 \tag{2.7a}$$

and

$$dv - Z_w di + R i dx = 0 \tag{2.7b}$$

The fact that system (2.1) is hyperbolic guarantees that every point in the $x-t$ plane is crossed only by one characteristic belonging to the family of solutions to (2.6a) and another one belonging to the family of solutions to (2.6b). Therefore, the characteristics curves obtained from (2.6a) and (2.6b) can be taken as a coordinate system in which equations (2.7a) and (2.7b) are equivalent to system (2.1) [9].

For their solution, (2.7a) and (2.7b) are discretized in space (x -coordinate) and time (t -coordinate) as shown in Fig. 2.1. Applying central differences, (2.7a) and (2.7b) yields:

$$(v^G - v^E) + Z_w (i^G - i^E) + \frac{\Delta x}{2} R (i^G + i^E) = 0 \tag{2.8a}$$

and

$$(v^G - v^F) - Z_w (i^G - i^F) - \frac{\Delta x}{2} R (i^G + i^F) = 0 \tag{2.8b}$$

Equations (2.8a) and (2.8b) give the solution for the variables v and i at point G of Fig. 2.1. Thus, voltages and currents for the internal nodes of the discretization mesh of Fig. 2.1 at time $t+\Delta t$ can be calculated from their known values at the previous time t . For a point at one of the line ends, only one characteristic insides on it thus providing a single equation of the type (2.8a) or (2.8b). The other equation needed to extend the solution to the corresponding point at the time $t+\Delta t$ has to be obtained from the line boundary conditions.

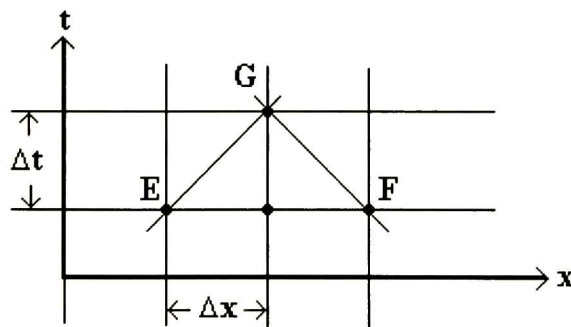


Fig. 2.1 Discretization mesh

2.3 Single-phase line with skin effect

When a wave propagates along a lossy line, its spectral components travel with different speeds and attenuations producing the distortion of the original waveshape. In overhead lines this is due to skin effect in the conductors and in the ground plane [11]. A model that considers this has been proposed by Radulet, *et. al.*, and is given by the following equations [11]:

$$\frac{\partial v}{\partial x} + L_o \frac{\partial i}{\partial t} + \frac{\partial}{\partial t} \int_0^t r'(t-\tau) i(\tau) d\tau = 0 \quad (2.9a)$$

and

$$\frac{\partial i}{\partial x} + C_o \frac{\partial v}{\partial t} + \frac{\partial}{\partial t} \int_0^t g'(t-\tau) v(\tau) d\tau = 0, \quad (2.9b)$$

where L_o and C_o are the geometric inductance and capacitance of the line, respectively; $r'(t)$ and $g'(t)$ are the transient longitudinal resistance and transient shunt conductance parameters, respectively. Usually, in the case of overhead transmission lines, one can neglect $g'(t)$; from here on, it will thus be omitted. The parameter $r'(t)$ is defined as the p.u.l. voltage drop at the periphery of the line conductor that appears after the injection of a current unit step $i = u(t)$ [11]:

$$r'(t) = - \left. \frac{\partial v}{\partial x} \right|_{i=u(t)} \quad t > 0 \quad (2.10)$$

This function is positive, monotonically decreasing and has the following limits [11]:

$$\lim_{t \rightarrow \infty} r'(t) = R_{dc} \quad \text{and} \quad \lim_{t \rightarrow 0} r'(t) = \infty \quad (2.11a, b)$$

In [16] $r'(t)$ is obtained analytically in terms of Bessel functions and of the complementary error function. These analytical expressions, however, are restricted to specific line geometry and do not permit accounting for the discontinuity of $r'(t)$ at $t = 0$. The method proposed as follows is applicable to any line geometry and deals with the discontinuity at $t = 0$ by including a term consisting in the convolution of the current with Dirac's impulse function.

2.3.1 Transient resistance in frequency domain

In [16] the transient resistance is obtained effectively from analytical expressions which are valid only for single-phase lines consisting of a cylindrical conductor and flat ground plane. A

frequency domain methodology to synthesize $r'(t)$ which is valid for any line configuration is developed as follows.

In the frequency domain, the first of the Telegrapher's equations is:

$$-\frac{dV}{dx} = [sL(s) + R(s)]I(s), \quad (2.12a)$$

where:

$$L(s) = L_o + L_c(s) + L_g(s) \quad \text{and} \quad R(s) = R_c(s) + R_g(s).$$

$L_g(s)$ and $R_g(s)$ are the inductance and resistance parameters due to ground, respectively; $L_c(s)$ and $R_c(s)$ are the conductor's internal inductance and resistance parameters, respectively. Applying Laplace transform to (2.9a) one obtains:

$$-\frac{dV}{dx} = [sL_o + sR'(s)]I(s) \quad (2.13)$$

Expressions (2.12a) and (2.13) should be equivalent; therefore:

$$R'(s) = \frac{Z_g(s) + Z_c(s)}{s}. \quad (2.14)$$

where:

$$Z_g(s) = R_g(s) + sL_g(s) \quad \text{and} \quad Z_c(s) = R_c(s) + sL_c(s).$$

For an overhead line $Z_g(s)$ and $Z_c(s)$ can be determined at different frequencies by using the concept of complex depth of images as described in [12]. With these values, it is possible to synthesize a linear network with constant parameters R and C [3] which approximates $R'(s)$. This network corresponds to a rational function of the type:

$$R'(s) \cong \frac{k_o}{s} + \sum_{l=1}^N \frac{k_l}{s + p_l} + k_\infty \quad (2.15)$$

where N is the order of the fit. Applying Laplace initial and final value theorems to (2.15):

$$\lim_{t \rightarrow \infty} r'(t) = \lim_{s \rightarrow 0} sR'(s) = k_o \quad \text{and} \quad \lim_{t \rightarrow 0} r'(t) = \lim_{s \rightarrow \infty} sR'(s) = \infty \quad (2.16a, b)$$

Expressions (2.16a) and (2.16b) coincide with (2.11a) and (2.11b), provided $k_o = R_{dc}$. Extracting the term that contains R_{dc} from (2.15), the remaining function to be synthesized is:

$$H(s) = R'(s) - \frac{k_o}{s} = \sum_{l=1}^N \frac{k_l}{s + p_l} + k_\infty \quad (2.17)$$

2.3.2 Transient resistance rational fitting

Both, the transient resistance $R'(s)$ and function $H(s)$ of (2.17) are non-rational functions that can be approximated by rational ones. A fitting method developed by J. Martí [13] is based on adapting Bode's asymptotic plots. Poles and zeros obtained through this method are real and the fit has the form:

$$H(s) \cong \frac{(s - z_1)(s - z_2) \cdots (s - z_n)}{(s - p_1)(s - p_2) \cdots (s - p_n)}, \quad (2.18)$$

where the z_l terms and the p_l terms (with $l = 1, \dots, N$) are real zeros and real poles, respectively. Another possibility is to use Padé's method which consists in considering the following expression:

$$H(s) = \frac{a_N s^N + \cdots + a_1 s + a_0}{b_N s^N + \cdots + b_1 s + 1} \quad (2.19)$$

Then (2.19) is evaluated at a certain number of frequencies to form an over-determined system of linear equations whose unknowns are the $2N+1$ coefficients. The solution of this system of equations generally yields complex poles and complex zeros. When real poles and zeros are desired, a method proposed for Kuznetsov and Schutt-Ainé can be applied [37]. In both, standard Padé and Kuznetsov methods, an over-determined system of equations of the following form is obtained:

$$\mathbf{M}\mathbf{x} = \mathbf{y} \quad (2.20)$$

System (2.20), finally, can be solved by least squares or by singular value decomposition [22].

When the frequency range of interest for a fit spans several decades, as usually is the case in electromagnetic transients computation, (2.20) can easily lead to an extremely ill-conditioned matrix \mathbf{M} . To avoid this numerical problem, the procedure proposed by Silveira, *et. al.*, can be used [31]. This method is based on dividing the complete range of frequencies $\Omega = [\Omega_{\min} \Omega_{\max}]$ in a number of non-overlapping sub-ranges $\Omega_1, \Omega_2, \dots, \Omega_w$, in such form that their union is Ω . Low order local approximations can thus be performed at each sub-range and then be incorporated into a global approximation scheme.

Recently, a very powerful method for approximating non-rational functions of frequency by means of rational functions has been introduced by Semlyen and Gustavsen. This method, referred to as Vector Fitting (VF), is very effective even if the original function presents several spikes [44]. The fitting methods of J. Martí, Padé, Silveira-Kuznetsov and VF are applied as follows in the synthesis of the $H(s)$ function for the line described by Fig. 2.2. This figure provides the plots of the fittings along with the original non-rational function $H(s)$. It is clear from Fig. 2.2 that Padé's method overweights higher frequency data yielding a poor accuracy at low frequencies. The number of real poles obtained with Martí's technique is 13. A 14th order approximation has been used for Padé's method. In the case of Silveira-Kuznetsov's method with local approximations, 13 real poles have been used and the frequency range has been divided in 6 sections. The fitting of $H(s)$ has been done with VF using 8 real poles and a *rms* error of 1.5×10^{-8} . The curves obtained with Silveira-Kuznetsov and VF methods are not shown in Fig. 2.2 since their differences with the original function are not distinguishable by eye.

In the previous example, VF has produced both the lowest order approximation (8 poles) and the lowest *rms* overall error. Lowering the approximation order is important for increasing the computational efficiency of transient simulations. In the past, the author of this thesis has applied a model order reduction technique based on balanced realizations [22]. Nevertheless, the most recent experience with VF is that it produces similar model orders and much less overall error.

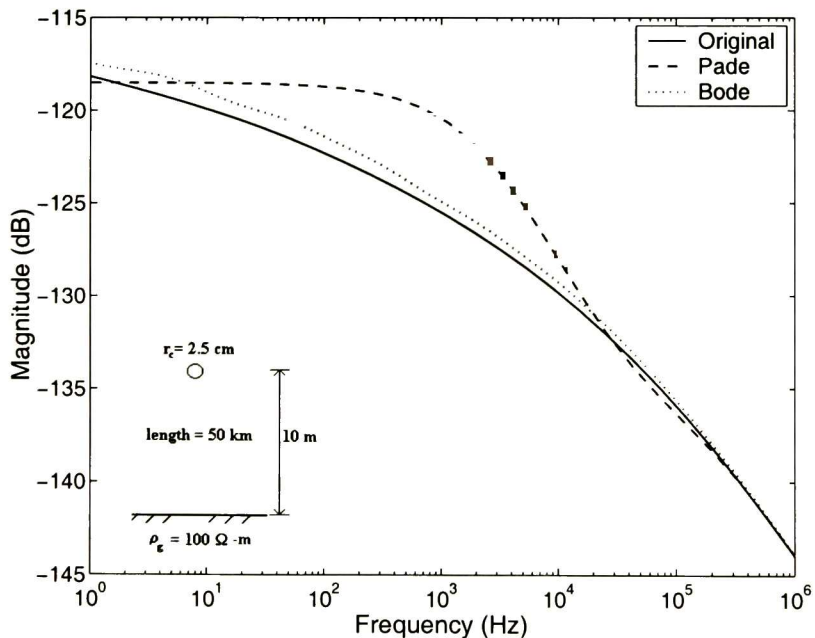


Fig. 2.2 Fitting of $H(s)$ for single-phase line example

2.4 Numerical convolution

The method of Characteristics described in section 2.2 can be extended to solve equations (2.9a) and (2.9b) for lines with frequency dependent parameters. This however requires a method to compute numerically the convolution terms. Such method is described as follows.

The time domain equivalent of (2.15) is:

$$r'(t) \equiv k_o u(t) + \sum_{l=1}^N k_l e^{-p_l t} + k_\infty \delta(t) \quad (2.21)$$

On introducing (2.21) in (2.9a), and after solving the convolutions corresponding to the step and the Dirac's delta terms, one obtains:

$$\frac{\partial v}{\partial x} + D \frac{\partial i}{\partial t} + R_{cd} i + \vartheta = 0 \quad (2.22a)$$

where:

$$D = L_o + k_\infty \quad (2.22b)$$

and

$$\vartheta = \frac{\partial}{\partial t} \int \sum_{l=1}^N k_l e^{p_l(t-\tau)} i(\tau) d\tau \quad (2.22c)$$

Since $g'(t)$ is neglected, expression (2.9b) becomes:

$$\frac{\partial i}{\partial x} + C_o \frac{\partial v}{\partial t} = 0 \quad (2.22d)$$

Expression (2.22c) involves the exponential terms of $r'(t)$ only; therefore, the recursive convolution method of Semlyen and Dabuleanu can be applied in its evaluation [10]. An alternative technique to implement this method is described next. In the Laplace domain, the convolution term in (2.22c) can be expressed as follows:

$$\Psi = \Psi_1 + \dots + \Psi_N, \quad (2.23a)$$

with:

$$\Psi_l = \frac{k_l}{s + p_l} I; \quad l = 1, \dots, N. \quad (2.23b)$$

On rearranging equation (2.23b) and converting it to time domain:

$$\frac{d\Psi_l}{dt} + p_l \Psi_l = k_l i; \quad l = 1, \dots, N. \quad (2.24)$$

where the ψ_l terms correspond to the inverse Laplace transforms of the Ψ_l ones. Equation (2.24) can be approximated by finite differences as follows:

$$\Psi_{l,m+1} = -\frac{\Delta t}{1 + p_l \Delta t} \left[\frac{\Psi_{l,m}}{\Delta t} + k_l i_{m+1} \right]; \quad l = 1, \dots, N. \quad (2.25)$$

where the sub-indexes m and $m+1$ correspond to samples at times $m\Delta t$ and $(m+1)\Delta t$, respectively.

Finally, the total convolution term ψ_{m+1} is obtained as follows:

$$\Psi_{m+1} = \sum_{l=1}^N \Psi_{l,m+1} = \sum_{l=1}^N \frac{\Delta t}{1 + p_l \Delta t} \left[\frac{\Psi_{l,m}}{\Delta t} + k_l i_{m+1} \right] \quad (2.26)$$

The method of Characteristics now is applied to (2.22a) and (2.22d), the following system of equations is thus obtained:

$$\lambda_{1,2} = \frac{dx}{dt} = \pm \frac{1}{\sqrt{DC}}, \quad (2.27a)$$

$$dv + Z_w di + R_{cd} i dx + \vartheta dx = 0 \quad (2.27b)$$

and

$$dv - Z_w di + R_{cd} i dx + \vartheta dx = 0 \quad (2.27c)$$

where ϑ is the term that groups the convolutions due to $r'(t)$. A discretized version of ϑ would simply be:

$$\vartheta_{m+1} = (\Psi_{m+1} - \Psi_m) / \Delta t \quad (2.27d)$$

The numerical solution scheme for (2.27a)-(2.27c) is practically the same as for the one in section 2.2, except for the terms involving ϑ which are readily incorporated by means of (2.25), (2.26) and (2.27d).

The previously described method of Characteristics, which includes convolutions, is applied now in the simulation of a linear double ramp wave (1V/10 μ s/90 μ s) being injected into the line described by Fig. 2.2. Figure 2.3 shows the simulated waveforms at various distances from the injection point. These waveforms are calculated also by means of the frequency domain method known as the Numerical Laplace Transform (NLT) [17]. One can observe in this figure the very close agreement between the two sets of plots. It should be mentioned that, for the numerical method of Characteristics, the line function $H(s)$ used is the one with 8 poles that was obtained in the previous section with the VF technique.

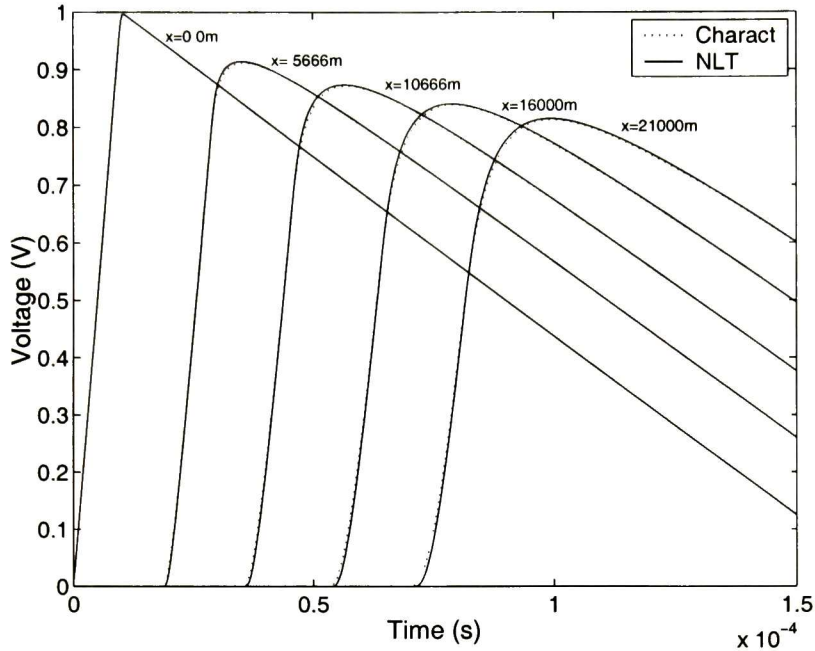


Fig. 2.3 Resulting voltage waveforms along the single-phase line example

2.5 Single-phase lines with corona and skin effects

When a line conductor voltage reaches certain critical value (v_{crit}), the electric field in the neighborhood becomes higher than the dielectric strength of the air and ionization is produced around the conductor. In this way, the ionized region presents storage and movement of charges. This phenomenon, known as corona effect, causes the line capacitance becoming a function of voltage and perhaps also of the time derivatives of this voltage [23]. A model of corona based on the physical microscopic processes would be very complicated and impractical for transient analysis of transmission lines. An example of this type of models has been developed by Abdel-Salam [20]. For transient analysis it is common to use models based on macroscopic descriptions of the corona phenomenon; for instance models based on voltage-charge curves ($q-v$ curves) [16]. For these models in which the corona capacitance is only function of the voltage, $C_{cor} = f(v)$, will be referred to hereafter as *static* models. On the other hand, when the corona capacitance is expressed as a function of voltage and its derivatives, $C_{cor} = f(v, \partial v/\partial t, \dots)$, it is said that the model is *dynamic* [23].

Corona models based on the q - v curves can be classified as piecewise linear, parabolic, dynamic, etc. In the former ones the q - v curves are approximated by straight lines. In the parabolic models, the corona capacitance is approximated by a generalized parabola. Dynamic models take into account the fact that the corona charge depends on the voltage and on its rate of change. The following parabolic model have been proposed by Gary, *et. al.* [23]. Since this model is derived from a large amount of experimental data, it is adopted here for representing the corona capacitance C_{cor} .

$$C_{cor} = \begin{cases} C_o & v \leq v_{crit}, \partial v / \partial t > 0 \\ C_o \beta \left(\frac{v}{v_{crit}} \right)^{\beta-1} & v > v_{crit}, \partial v / \partial t > 0 \\ C_o & \partial v / \partial t \leq 0 \end{cases} \quad (2.28)$$

In this model, v_{crit} is obtained by means of the well-known formula by Peek [32], r_c is the conductor radius in centimeters and β is a parameter that depends on the number of the bundle conductors and on the voltage polarity. For a single conductor with positive voltage polarity [32]:

$$\beta = 0.22 r_c + 1.2 \quad (2.29)$$

Equations (2.27a)-(2.27c) are applicable to describing wave propagation including corona. One has to bear in mind that now λ and Z_w are functions of voltage; that is:

$$\lambda_{1,2} = \frac{dx}{dt} = \pm \frac{1}{\sqrt{DC(v)}} \quad (2.30)$$

and

$$Z_w(v) = \sqrt{D / C(v)} \quad (2.31)$$

where D is the inductance defined by (2.22b).

For linear lines, the characteristics are straight lines with constant slopes. This is the case for the example provided in section 2.4. It now follows from (2.30) that, for non-linear lines, the characteristics generally are curves which depend on the solution of the line PDEs. Since these two PDEs constitute a hyperbolic system, the corresponding characteristics still provides a solution coordinate system [9], albeit a distorted one. The straight implementation of (2.27b), (2.27c), (2.30) and (2.31) using finite differences would thus result in a highly irregular discretization mesh in the x - t plane. A more convenient finite differences implementation which produces a regular discretization mesh is described in [32]. It consists in prescribing fixed values

for Δx and Δt in such manner that the Courant-Friedrichs-Lewy (CFL) condition always be satisfied [27]:

$$\Delta x/\Delta t = 1/\sqrt{DC} \quad (2.32)$$

The characteristics then are forced to coincide with the mesh nodes by applying interpolations. The details of the method are given in [32].

Equations (2.27b), (2.27c), (2.30) and (2.31) are now applied, along with the regular mesh finite difference method, in the simulation of a field experiment conducted by Wagner, *et. al.* [1]. This experiment consisted in the injection of an almost double exponential impulse (1560kV/0.35 μ s/6 μ s) at the beginning of a short line section with a corona inception voltage at 400kV. For simulation purposes, it is assumed that the line is a single-phase one. In addition, the following data are used: conductor radius $r_c = 2.54$ cm, conductor medium height $h = 20.72$ m, conductor material in aluminum, earth resistivity $\rho_g = 100$ Ω -m, line length $l = 2185.4$ m, line termination $R_{load} = 400$ Ω .

Figure 2.4a shows the experimental measurements by Wagner, *et. al.* [1], Fig. 2.4b shows the simulation results obtained here. The latter figure shows the effect of corona on the traveling impulse both, with and without frequency dependence considerations. The simulation without frequency dependence had been accomplished and reported previously in [32]. The comparison between 2.4a and 2.4b shows that the inclusion of frequency dependence yields results that are closer to the measured values. There are, however, still noticeable differences between simulated and experimental results. They are attributed here mostly to the following factors:

- a) In the simulation corona is represented by a static model instead of by a dynamic model.
- b) For the real line, the conductor height varies between towers from 15.24m to 26.2m.
- c) The real multiconductor system is formed by two horizontal three-phase lines and their respective ground wires; while the simulated is assumed as a single-phase line.
- d) The simulation considered a cylindrical conductor and, since the earth resistivity was not reported in [1], it is assumed here as 100 Ω -m.

Concerning item b), it implies that the simulation excluded non-uniform line effects as well as the fact that corona inception voltage is affected by changes of the conductor height.

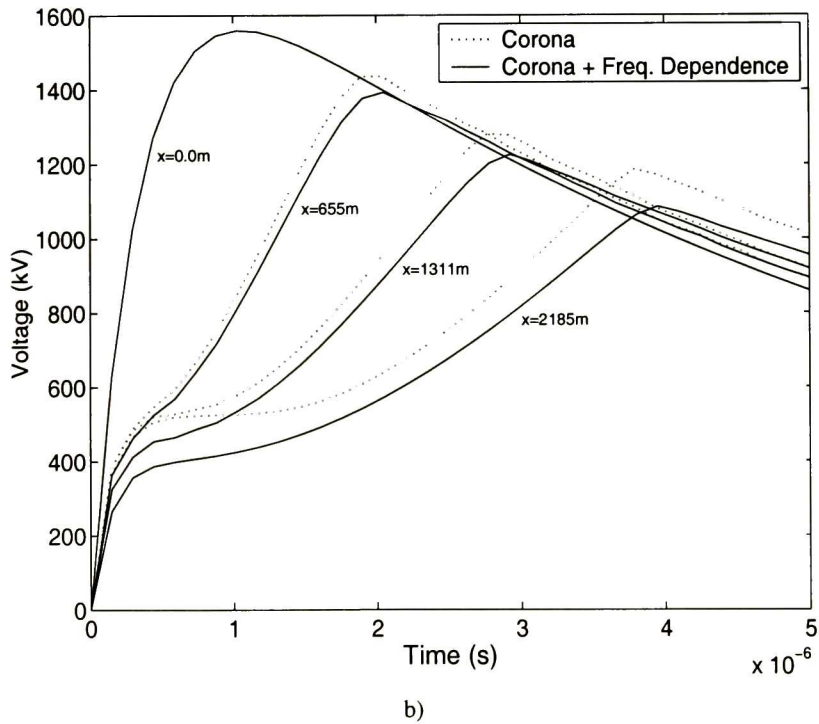
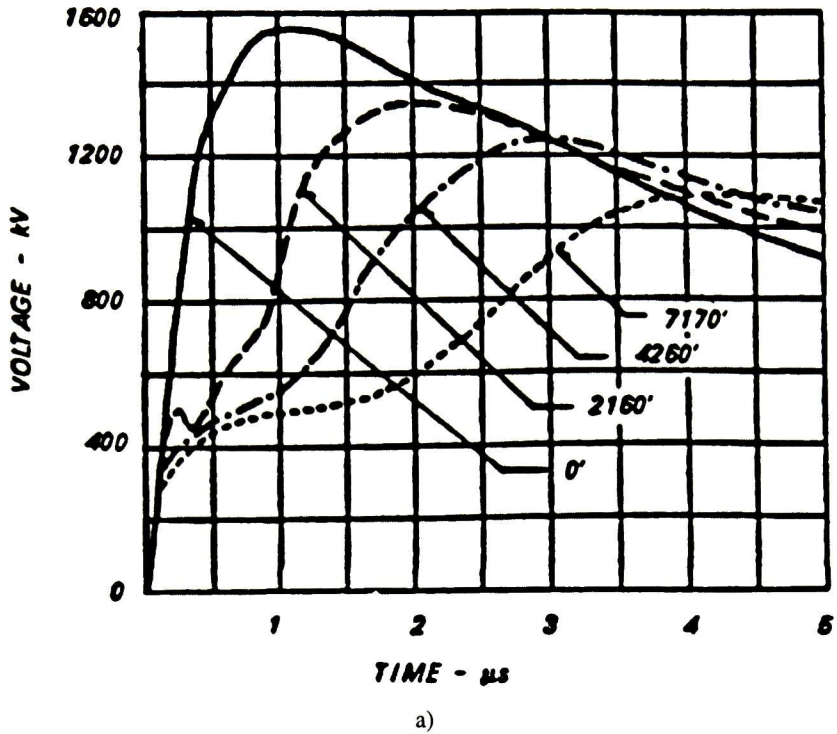
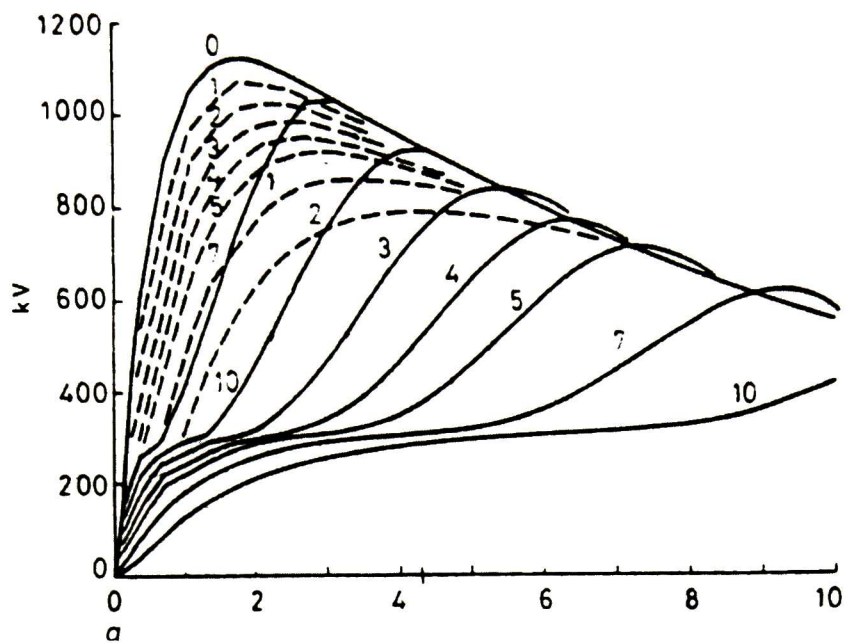
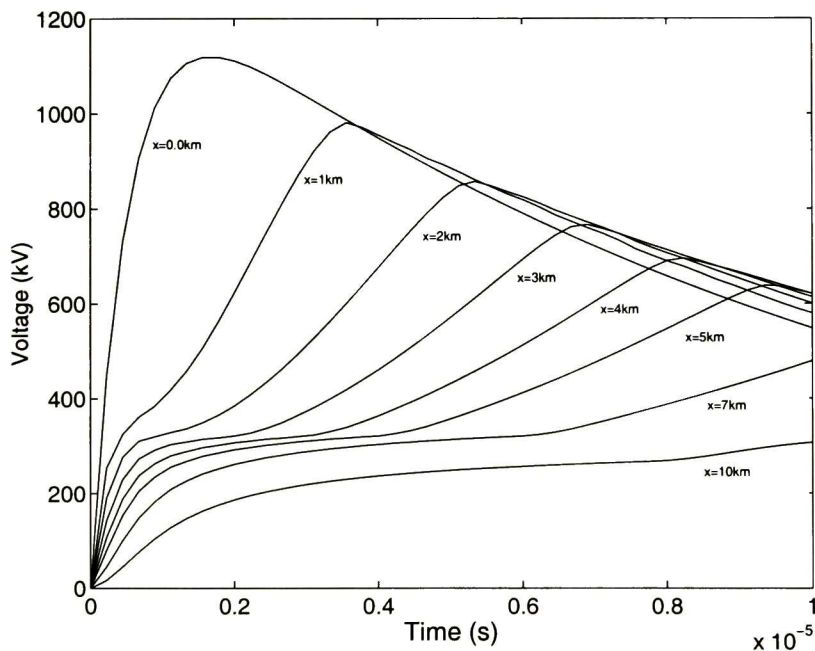


Fig. 2.4 a) Wagner's experiment waveforms, and b) Characteristics' simulation waveforms



a)



b)

Fig. 2.5 a) Gary's model simulation waveforms, and b) Characteristics' simulation waveforms

A second application example for the method proposed here is the reproduction of simulations by Gary, *et. al.* [16]. Assume a uniform single-phase transmission line, 10 km long, conformed by a cylindrical conductor with 1.32 cm radius, located 12 m above a ground plane with a 100 Ω -m resistivity. The line is terminated with a 450 Ω resistance and, at the other end, a (1120kV/0.524 μ s/10.9 μ s) double exponential impulse is injected. The critical voltage for this line is assumed at 320 kV. Figure 2.5a shows the results obtained by Gary, *et. al.*, in [16]. Notice that wave tails are not provided. Figure 2.5b shows the results obtained with the simulation method proposed here. Notice the coincidence of the wave fronts in both simulations.

2.6 Remarks

A method for calculating electromagnetic transients in overhead transmission lines taking into account linear and non-linear dispersion has been presented. The propagation equations with transient parameters and non-linear effects have been solved by means of the method of Characteristics. This method eliminates the numerical oscillations usually encountered in methods using other spatial discretization techniques. The method further can be extended to multiconductor and to non-quasi-linear line cases. The frequency dependence of line parameters has been included by means of a convolution procedure based in a synthesized rational function. The non-linear characteristic due to corona effect is included by means of an iterative process in the finite difference solution of the transmission line equations. The method has been validated by comparison with experimental results and it has been shown that the proposed model correctly predicts the main properties of the waveforms.

III MULTICONDUCTOR LINEAR LINE MODELING IN TIME DOMAIN INCLUDING FREQUENCY DEPENDENCE EFFECT

3.1 Introduction

Over the last 30 years, considerable efforts have been devoted by various specialists towards the development of a time domain full frequency dependent multiconductor line model. The following references provide only a very partial list of these efforts: [7, 8, 10, 13, 21, 41, 42, 44, 45, 36]. An idempotent decomposition method introduced by Wedepohl [15] has served as basis for a recent traveling wave type model. This new model has succeeded in effectively decoupling modal travel delays [35, 39, 43, 45].

Apart from traveling wave methods, one can use finite differences to produce a multiconductor line model, that is in time domain and include full frequency dependent effects. Traveling wave methods are perhaps more effective for producing long homogeneous line section models. There are cases, however, in which lines have to be subdivided and, thus, a finite difference based model could be more convenient. A few examples of these cases are: 1) lines excited by distributed sources, 2) underground cables with multiple cross-bondings, 3) non-uniform lines and 4) lines with distributed non-linearities as corona.

A new finite differences line model is presented in this chapter. It is based on the multiconductor line equations by Radulet, *et. al.* [11], as well as on the method of Characteristics of PDE theory [9]. The advantages of this model with respect to traveling wave type models are stressed here for cases in which lines have to be subdivided. The new model is applied to a case consisting in a distribution line being excited by an externally radiated electromagnetic (EM) field. The new model is also applicable to long homogeneous sections of line or cable, although for this case the model is computationally less efficient than traveling wave models. Two additional application cases involving long line sections are provided here. One consists in a transient on a highly asymmetric overhead line. The other consists in the transient simulation of an underground cable.

3.2 Telegrapher's equations for lines with frequency dependent parameters

For a n -phase transmission line or cable, the modified Telegrapher's equations proposed by Radulet, *et. al.*, can be expressed as follows [11]:

$$\frac{\partial \mathbf{v}}{\partial x} + \mathbf{L}_o \frac{\partial \mathbf{i}}{\partial t} + \frac{\partial}{\partial t} \int_0^t \mathbf{r}'(t - \tau) \mathbf{i}(\tau) d\tau = 0 \quad (3.1a)$$

and

$$\frac{\partial \mathbf{i}}{\partial x} + \mathbf{C}_o \frac{\partial \mathbf{v}}{\partial t} + \frac{\partial}{\partial t} \int_0^t \mathbf{g}'(t - \tau) \mathbf{v}(\tau) d\tau = 0 \quad (3.1b)$$

where \mathbf{L}_o is the geometric inductances matrix of the line, \mathbf{C}_o is its matrix of geometric capacitances [12], $\mathbf{r}'(t)$ is its matrix of transient series resistances and $\mathbf{g}'(t)$ is its matrix of transient shunt conductances. All these matrices are of dimension $n \times n$. As in the case of single-phase overhead lines, matrix $\mathbf{g}'(t)$ usually is neglected. Since this does not imply any loss of generality, instead of (3.1b) the following expression is hereafter used:

$$\frac{\partial \mathbf{i}}{\partial x} + \mathbf{C}_o \frac{\partial \mathbf{v}}{\partial t} = 0 \quad (3.1c)$$

In a similar fashion as for single-phase lines, $\mathbf{r}'(t)$ has the following limits:

$$\lim_{t \rightarrow \infty} \mathbf{r}'(t) = \text{diag}\{R_{dc,1}, R_{dc,2}, \dots, R_{dc,n}\} \quad \text{and} \quad \lim_{t \rightarrow 0} \mathbf{r}'(t) = (\infty)_{n \times n} \quad (3.2a, b)$$

where $R_{dc,q}$, $q = 1, 2, \dots, n$, is the direct current resistance of the q -th conductor, and $(\infty)_{n \times n}$ is an $n \times n$ square matrix whose elements are infinite. By following essentially the same procedure as in section 2.3.1, one can arrive at the following relationship between $\mathbf{R}'(s)$, the Laplace domain image of $\mathbf{r}'(t)$, and $\mathbf{Z}_g(s)$ and $\mathbf{Z}_c(s)$, the Laplace domain matrices of earth and of conductor impedances, respectively [12].

$$\mathbf{R}'(s) = \frac{1}{s} [\mathbf{Z}_g(s) + \mathbf{Z}_c(s)] \quad (3.3)$$

Each one of the elements of $\mathbf{R}'(s)$ is a non-rational function of s and, in addition, $\mathbf{R}'(s)$ is symmetric. Since lines are made of good conductors and the earth usually is a bad conductor, it is expected that the $\mathbf{Z}_g(s)$ term of (3.3) dominates upon $\mathbf{Z}_c(s)$. In addition, all the elements in $\mathbf{Z}_g(s)$ result from the same skin effect on the earth. These two considerations suggest that all the

different elements of $\mathbf{R}'(s)$ can be fitted with rational functions using the same set of poles. In this author's experience, this has always been the case; therefore:

$$\mathbf{R}'(s) \cong \frac{1}{s} \mathbf{k}_o + \mathbf{k}_\infty + \sum_{l=1}^N \frac{1}{s - p_l} \mathbf{k}_l \quad (3.4)$$

where N is the order of the fit, \mathbf{k}_o is the matrix of residues of $\mathbf{R}'(s)$ at $s = \infty$, \mathbf{k}_∞ is its residues matrix at $s = 0$ and \mathbf{k}_l ($l = 1, \dots, N$) is its residues matrix at $s = p_l$ [3]. Notice from (3.4) and (3.2a) that:

$$\mathbf{k}_o = \text{diag}\{R_{dc,1}, R_{dc,2}, \dots, R_{dc,n}\}. \quad (3.5)$$

Consider next the time domain image of (3.4):

$$\mathbf{r}'(t) \cong \mathbf{k}_o u(t) + \mathbf{k}_\infty \delta(t) + \sum_{l=1}^N e^{p_l t} \mathbf{k}_l \quad (3.6)$$

On applying (3.6) in (3.1a), one obtains:

$$\frac{\partial \mathbf{v}}{\partial x} + \mathbf{D} \frac{\partial \mathbf{i}}{\partial t} + \mathbf{k}_o \mathbf{i} + \frac{\partial}{\partial t} \int_0^t \mathbf{h}(t - \tau) \mathbf{i}(\tau) d\tau = 0, \quad (3.7)$$

where

$$\mathbf{h}(t) = \sum_{l=2}^N e^{p_l t} \mathbf{k}_l \quad (3.8)$$

and

$$\mathbf{D} = \mathbf{L}_o + \mathbf{k}_\infty. \quad (3.9)$$

Expressions (3.1c) and (3.7) constitute the basis of the line model proposed in this chapter.

3.3 Transmission line equations and Characteristics

A multiconductor line model based on Characteristics has been already developed in [28] for the frequency independent line case. The method of Characteristics of PDE Theory is applied next to (3.1c) and (3.7) for a full frequency dependent model of multiconductor lines. Consider the following form of (3.7):

$$\frac{\partial \mathbf{v}}{\partial x} + \mathbf{D} \frac{\partial \mathbf{i}}{\partial t} + \mathbf{k}_o \mathbf{i} + \boldsymbol{\theta} = 0, \quad (3.10)$$

where

$$\boldsymbol{\theta} = \frac{\partial}{\partial t} \int_0^t \mathbf{h}(t - \tau) \mathbf{i}(\tau) d\tau.$$

Equations (3.1c) and (3.10) can be grouped as:

$$\frac{\partial}{\partial t} \mathbf{u} + \mathbf{A} \frac{\partial}{\partial x} \mathbf{u} + \mathbf{B} \mathbf{u} + \mathbf{f} = \mathbf{0}, \quad (3.11)$$

where:

$$\mathbf{u} = \begin{bmatrix} \mathbf{v} \\ \mathbf{i} \end{bmatrix} \quad \mathbf{A} = \begin{bmatrix} \mathbf{0} & \mathbf{C}_o^{-1} \\ \mathbf{D}^{-1} & \mathbf{0} \end{bmatrix} \quad \mathbf{B} = \begin{bmatrix} \mathbf{0} & \mathbf{0} \\ \mathbf{0} & \mathbf{D}^{-1} \mathbf{k}_o \end{bmatrix} \quad \text{and} \quad \mathbf{f} = \begin{bmatrix} \mathbf{0} \\ \mathbf{D}^{-1} \boldsymbol{\theta} \end{bmatrix}.$$

Note the similarity between (2.1) and (3.11). The latter is a 1st order hyperbolic system provided \mathbf{A} has real eigenvalues and $2n$ linearly independent eigenvectors; that is, \mathbf{A} is similar to a real diagonal matrix. The proof of this being always the case is given in [28].

Matrix products $\mathbf{D} \mathbf{C}_o$ and $\mathbf{C}_o \mathbf{D}$ also are always diagonalizable [28]. Let \mathbf{T}_v and \mathbf{T}_i be the matrices that diagonalize these products as follows:

$$\mathbf{T}_v^{-1} \mathbf{D} \mathbf{C}_o \mathbf{T}_v = \Lambda \quad (3.12a)$$

and

$$\mathbf{T}_i^{-1} \mathbf{C}_o \mathbf{D} \mathbf{T}_i = \Lambda \quad (3.12b)$$

\mathbf{T}_v can be interpreted as a matrix of column modes of voltage for a line with the following constant parameters:

$$\mathbf{L} = \mathbf{D} = \mathbf{L}_o + \mathbf{k}_\infty, \quad \mathbf{C} = \mathbf{C}_o \quad \text{and} \quad \mathbf{R} = \mathbf{0}.$$

Similarly, \mathbf{T}_i would be the matrix of current mode columns for this line. The nonzero elements of diagonal Λ are positive and equal to the square inverses of the corresponding modal propagation velocities. The following modal quantities are next defined:

$$\mathbf{v} = \mathbf{T}_v \mathbf{v}_m \quad \text{and} \quad \mathbf{i} = \mathbf{T}_i \mathbf{i}_m \quad (3.13a, b)$$

From (3.13a) and (3.13b), in modal domain (3.1c) and (3.10) become:

$$\frac{\partial \mathbf{v}_m}{\partial x} + \mathbf{D} \frac{\partial \mathbf{i}_m}{\partial t} + \mathbf{k}_o \mathbf{i}_m + \mathbf{T}_v^{-1} \boldsymbol{\theta} = \mathbf{0} \quad (3.14a)$$

and

$$\frac{\partial \mathbf{i}_m}{\partial x} + \mathbf{C}_o \frac{\partial \mathbf{v}_m}{\partial t} = \mathbf{0}, \quad (3.14b)$$

where:

$$\mathbf{D} = \mathbf{T}_v^{-1} \mathbf{D} \mathbf{T}_i \quad (3.15a)$$

$$\mathbf{C}_o = \mathbf{T}_i^{-1} \mathbf{C}_o \mathbf{T}_v \quad (3.15b)$$

$$\mathbf{k}_o = \mathbf{T}_v^{-1} \mathbf{k}_o \mathbf{T}_i. \quad (3.15c)$$

It can be shown that \mathbf{D} and $\tilde{\mathbf{C}}_o$ are diagonal, and further [28]:

$$\mathbf{\Lambda} = \mathbf{D}\tilde{\mathbf{C}}_o = \tilde{\mathbf{C}}_o\mathbf{D} \quad (3.16)$$

Two additional diagonal matrices are defined as:

$$\mathbf{\Gamma} = \sqrt{\mathbf{\Lambda}^{-1}} = \sqrt{\mathbf{D}^{-1}\tilde{\mathbf{C}}_o^{-1}} \quad (3.17a)$$

and

$$\mathbf{Z}_w = \sqrt{\mathbf{D}\tilde{\mathbf{C}}_o^{-1}} \quad (3.17b)$$

where $\mathbf{\Gamma}$ is the modal velocities matrix and \mathbf{Z}_w is the modal wave impedances matrix.

To apply the method of Characteristics in a straightforward manner, (3.1c) and (3.10) are first left multiplied by $\mathbf{\Gamma}$:

$$\mathbf{\Gamma} \frac{\partial \mathbf{v}_m}{\partial x} + \mathbf{Z}_w \frac{\partial \mathbf{i}_m}{\partial t} + \mathbf{\Gamma} \tilde{\mathbf{k}}_o \mathbf{i}_m + \mathbf{\Gamma} \mathbf{T}_v^{-1} \boldsymbol{\vartheta} = \mathbf{0} \quad (3.18a)$$

and

$$\frac{\partial \mathbf{v}_m}{\partial t} + \mathbf{\Gamma} \mathbf{Z}_w \frac{\partial \mathbf{i}_m}{\partial x} = \mathbf{0} \quad (3.18b)$$

Note that the following identity has been used in (3.18b):

$$\mathbf{\Gamma} \mathbf{Z}_w = \tilde{\mathbf{C}}_o^{-1} \quad (3.19)$$

Then, adding and subtracting (3.18b) to (3.18a):

$$\left(\frac{\partial}{\partial t} + \mathbf{\Gamma} \frac{\partial}{\partial x} \right) \mathbf{v}_m + \mathbf{Z}_w \left(\frac{\partial}{\partial t} + \mathbf{\Gamma} \frac{\partial}{\partial x} \right) \mathbf{i}_m + \mathbf{\Gamma} \tilde{\mathbf{k}}_o \mathbf{i}_m + \mathbf{\Gamma} \mathbf{T}_v^{-1} \boldsymbol{\vartheta} = \mathbf{0} \quad (3.20a)$$

and

$$\left(\frac{\partial}{\partial t} - \mathbf{\Gamma} \frac{\partial}{\partial x} \right) \mathbf{v}_m - \mathbf{Z}_w \left(\frac{\partial}{\partial t} - \mathbf{\Gamma} \frac{\partial}{\partial x} \right) \mathbf{i}_m - \mathbf{\Gamma} \tilde{\mathbf{k}}_o \mathbf{i}_m - \mathbf{\Gamma} \mathbf{T}_v^{-1} \boldsymbol{\vartheta} = \mathbf{0} \quad (3.20b)$$

Expression (3.20a) contains n equations of the following form:

$$\left(\frac{\partial}{\partial t} + \gamma_l \frac{\partial}{\partial x} \right) v_{m,l} + Z_{w,l} \left(\frac{\partial}{\partial t} + \gamma_l \frac{\partial}{\partial x} \right) i_{m,l} + \gamma_l \sum_{q=1}^n \tilde{k}_{o,lq} i_{m,q} + \gamma_l \sum_{q=1}^n T_{v,lq}^{-1} \vartheta_q = 0; \quad l = 1, \dots, n, \quad (3.21a)$$

where γ_l and $Z_{w,l}$ denote the respective l -th diagonal elements of $\mathbf{\Gamma}$ and \mathbf{Z}_w ; $\tilde{k}_{o,lq}$ and $T_{v,lq}^{-1}$ represent the respective elements of $\tilde{\mathbf{k}}_o$ and \mathbf{T}_v^{-1} at row l and at column q ; finally, $i_{m,l}$, $v_{m,l}$ and ϑ_l denote the l -th elements of the respective vectors \mathbf{i}_m , \mathbf{v}_m and $\boldsymbol{\vartheta}$. On the other hand, expression (3.20b) has n equations of the form:

$$\left(\frac{\partial}{\partial t} - \gamma_l \frac{\partial}{\partial x} \right) v_{m,l} - Z_{w,l} \left(\frac{\partial}{\partial t} - \gamma_l \frac{\partial}{\partial x} \right) i_{m,l} - \gamma_l \sum_{q=1}^n \tilde{k}_{o,lq} i_{m,q} - \gamma_l \sum_{q=1}^n T_{v,lq}^{-1} \vartheta_q = 0; \quad l = 1, \dots, n. \quad (3.21b)$$

Next, equations of the form (3.21a) are restricted to the corresponding characteristic curves of the x - t plane defined by:

$$\gamma_l = dx/dt; \quad l = 1, \dots, n. \quad (3.22)$$

Equation (3.21a) becomes thus:

$$dv_{m,l} + Z_{w,l} di_{m,l} + \gamma_l dt \sum_{q=1}^n \tilde{k}_{o,lq} i_{m,q} + \gamma_l dt \sum_{q=1}^n T_{v,lq}^{-1} \vartheta_q = 0; \quad l = 1, \dots, n. \quad (3.23)$$

As for equations (3.21b), these also are restricted to their corresponding characteristics curves defined by:

$$\gamma_l = -dx/dt; \quad l = 1, \dots, n, \quad (3.24)$$

thus becoming:

$$dv_{m,l} - Z_{w,l} di_{m,l} - \gamma_l dt \sum_{q=1}^n \tilde{k}_{o,lq} i_{m,q} - \gamma_l dt \sum_{q=1}^n T_{v,lq}^{-1} \vartheta_q = 0; \quad l = 1, \dots, n. \quad (3.25)$$

Expressions (3.22)-(3.25) provide $4n$ ordinary differential equations (ODEs) that are equivalent to the $2n$ PDEs provided by (3.1c) and (3.10).

3.4 Numerical solution of line equations

The Characteristics based finite difference method of section 2.4 is extended now to the frequency dependent and multiconductor line case represented by (3.22)-(3.25). Figure 3.1 illustrates a predetermined regular mesh in the x - t plane. As in the single-phase line case, Δt is determined from the Nyquist frequency and Δx must comply the CFL condition [27]. In the multiconductor case, however, there are n conditions or positive velocities; *i.e.* n positive characteristics passing through each (x, t) point. See for instance point G in Fig. 3.1. Clearly, Δx must be chosen as:

$$\Delta x = \gamma_{max} \Delta t, \quad (3.26)$$

with $\gamma_{max} = \max(\gamma_1, \dots, \gamma_n)$.

Suppose that line solutions are known at points E_1 and F_1 of Fig. 3.1 and that are to be extended to point G along the n positive and n negative characteristics. On applying central differences to (3.23) and (3.25):

$$\left(v_{m,l}^G - v_{m,l}^{E_l}\right) + Z_{w,l}\left(i_{m,l}^G - i_{m,l}^{E_l}\right) + \frac{\Delta x_l}{2} \sum_{q=1}^n \tilde{k}_{o,lq}\left(i_{m,q}^G + i_{m,q}^{E_l}\right) + \frac{\Delta x_l}{2} \sum_{q=1}^n T_{v,lq}^{-1}\left(\vartheta_q^G + \vartheta_q^{E_l}\right) = 0 \quad (3.27a)$$

and

$$\left(v_{m,l}^G - v_{m,l}^{F_l}\right) - Z_{w,l}\left(i_{m,l}^G - i_{m,l}^{F_l}\right) - \frac{\Delta x_l}{2} \sum_{q=1}^n \tilde{k}_{o,lq}\left(i_{m,q}^G + i_{m,q}^{F_l}\right) - \frac{\Delta x_l}{2} \sum_{q=1}^n T_{v,lq}^{-1}\left(\vartheta_q^G + \vartheta_q^{F_l}\right) = 0 \quad (3.27b)$$

with $\Delta x_l = \gamma_l \Delta t$ and with $l = 1, \dots, n$. Expressions (3.27a) and (3.27b) provide $2n$ equations for the $2n$ unknowns $v_{m,1}, \dots, v_{m,n}, i_{m,1}, \dots, i_{m,n}$. However, an issue that still has to be addressed is the one of evaluating convolution term ϑ . Consider the vector ϑ of dimension $n \times 1$ corresponding to the partial derivative of the convolution in (3.10) expressed as follows:

$$\vartheta(t) = \frac{\partial}{\partial t} \psi(t) \quad (3.28a)$$

with

$$\psi(t) = \int_0^t \mathbf{h}(t - \tau) \mathbf{i}(\tau) d\tau \quad (3.28b)$$

In the frequency domain, (3.28b) becomes:

$$\Psi(s) = \mathbf{H}(s) \mathbf{I}(s), \quad (3.28c)$$

where:

$$\mathbf{H}(s) = \sum_{l=1}^N \frac{1}{s - p_l} \mathbf{k}_l \quad (3.28d)$$

is the Laplace image of (3.8a). Let $\Psi(s)$ of (3.28c) be decomposed as:

$$\Psi = \Psi_1 + \dots + \Psi_N, \quad (3.29)$$

with:

$$\Psi_l = \frac{1}{s - p_l} \mathbf{k}_l \mathbf{I}; \quad l = 1, \dots, N \quad (3.30)$$

On passing (3.30) to the time domain:

$$\frac{d}{dt} \psi_l - p_l \psi_l = \mathbf{k}_l \mathbf{i}; \quad l = 1, \dots, N \quad (3.31)$$

and on applying finite differences to (3.31):

$$\psi_{l,m+1} = \frac{\Delta t}{1 - p_l \Delta t} \left(\frac{1}{\Delta t} \psi_{l,m} + \mathbf{k}_l \mathbf{i}_{m+1} \right); \quad l = 1, \dots, N \quad (3.32)$$

The term $\psi_{l,m+1}$ in (3.32) represents the l -th numerical convolution at $t = (m+1)\Delta t$. The total convolution for (3.28b) is:

$$\psi_{m+1} = \sum_{l=1}^N \frac{\Delta t}{1 - p_l \Delta t} \left(\frac{1}{\Delta t} \psi_{l,m} + \mathbf{k}_l \mathbf{i}_{m+1} \right) \quad (3.33)$$

Finally, (3.28a) is approximated numerically as:

$$\vartheta = \frac{\partial}{\partial t} \psi \cong \frac{1}{\Delta t} (\psi_{m+1} - \psi_m) \quad (3.34)$$

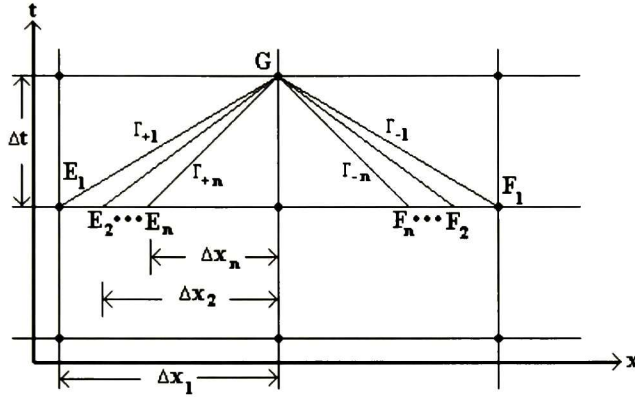


Fig. 3.1 Discretization mesh

3.5 Application examples

The previously proposed characteristics based line model is intended for the simulation of cases where lines have to be subdivided. Nevertheless, this model is applicable to long lines as well. The validation of this model is conducted next by applying it to three test cases. The first one corresponds to an overhead line excited by a distributed source. The second one involves a highly asymmetric overhead line. The third one is an underground transmission cable system. Cases two and three correspond to long line applications and their results are validated by means of the NLT technique. Case one requires line subdivision and is validated by means of the EMTP.

A) Illuminated distribution line

Figure 3.2 shows the geometry of a distribution line that is to be excited by EM field determined by the electric field intensity equal to a uniform linear double ramp [1(V/m)/10μs/90μs] propagating in the $-y$ direction. At end A , each conductor is grounded through a resistance $R_{load} = 400 \Omega$ and at end B the three conductors are left open.

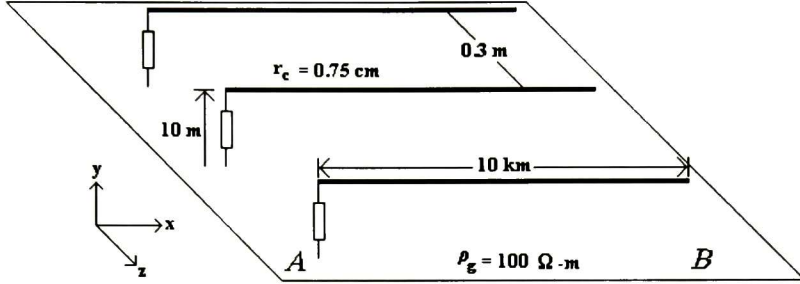


Fig. 3.2 Configuration for illuminated transmission line

To obtain the voltage waveforms at ends A and B through the Characteristics model, the following two terms should be added, respectively, to (3.1c) and (3.9) [5]:

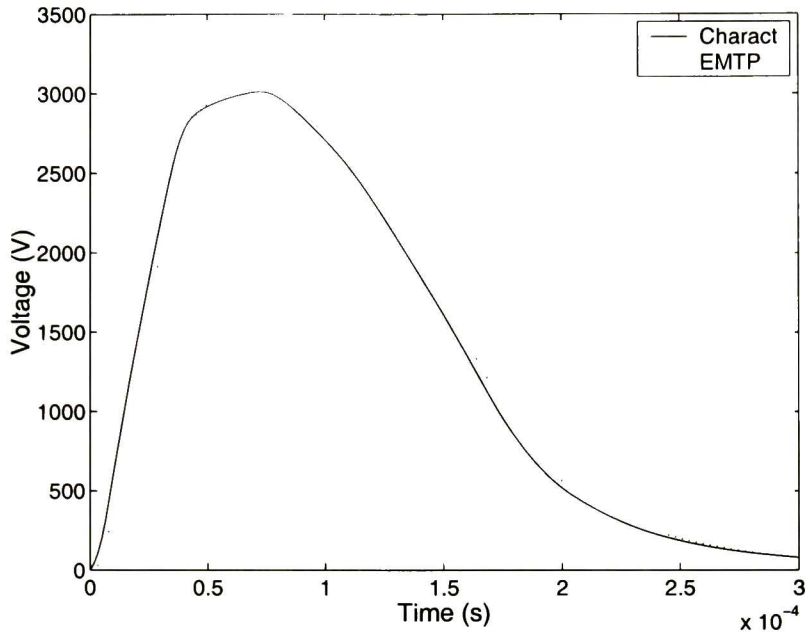
$$\mathbf{i}_p = -C_o \frac{\partial}{\partial t} \int_o^h \mathbf{E}_y^{inc} dy \quad (3.36a)$$

and

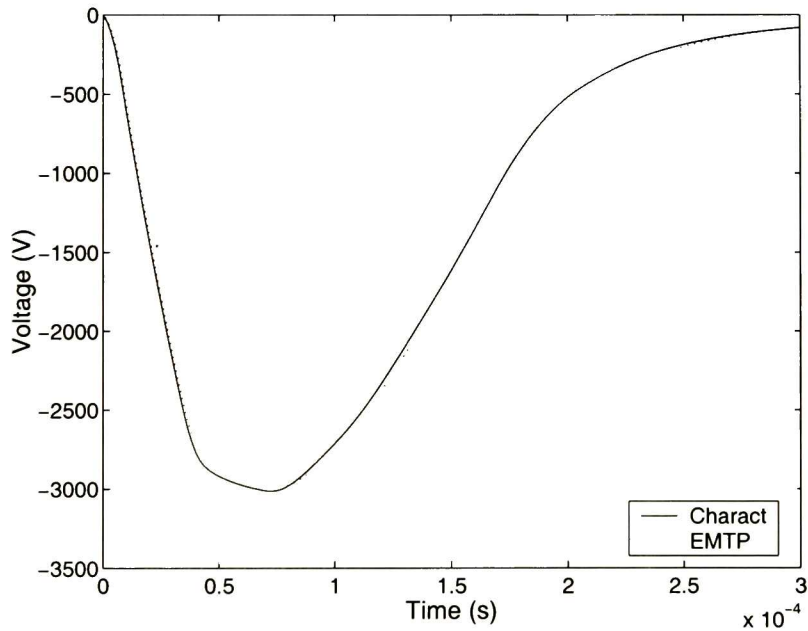
$$\mathbf{v}_s = \frac{\partial}{\partial t} \int_o^h \mathbf{B}_z^{inc} dy \quad (3.36b)$$

In equations (3.36a) and (3.36b) h is the corresponding conductor height above ground, \mathbf{B}_z^{inc} is the incident magnetic flux density in the z direction and \mathbf{E}_y^{inc} is the electrical field intensity in the y direction (being equal to zero in this application). To obtain the voltage waveforms using EMTP, the line is subdivided and equivalent sources are inserted between sections. Details of this are given in [34].

Figures 3.3a and 3.3b provide the voltage waveforms calculated for the central conductor at ends A and B , respectively. Both, the EMTP (Martí Setup) and the Characteristics model were used and, for both methods, the line was subdivided in 20 sections of length $\Delta x = 500$ m. The shift between Characteristics and EMTP shown in Fig. 3.3b is decreased when in the latter the line is subdivided in a larger number of sections. Further experiments showed that decreasing Δx in EMTP results in waveforms closer with those of Characteristics.



a)



b)

Fig. 3.3 Voltages induced at the ends of the central phase for illuminated distribution line

a) side A, b) side B

B) Highly asymmetric overhead line

Figure 3.4 depicts the transversal geometry of a highly asymmetric transmission system. It consists of two 100 km long transmission lines that run parallel 80 m apart one from the other. The first line is a double circuit vertical one, the second line is a single circuit horizontal one. The ground is considered homogeneous with resistivity $\rho_g = 100 \Omega\text{-m}$. At one extreme of this system (the sending end) conductor 1 is excited with a unit voltage step, while conductors 2 to 9 are grounded. At the receiving end, 100 km away, all the conductors are open. Figure 3.5 shows three waveforms at the receiving end as calculated with both, the time domain model proposed here and the NLT method. The NLT results were obtained considering 1024 samples along the observation time $t_{obs} = 20$ ms. As for the Characteristics results, the line was divided in 35 sections of length $\Delta x = 2857.1$ m. Figures 3.5a and 3.5b provide the voltage at the receiving end for conductors 1 and 6. In these two cases the agreement between the proposed model and the NLT method is remarkable. Figure 3.5c corresponds to conductor 9 of the unenergized line which is 80 m apart. Here, the difference between the two results are more noticeable; nevertheless, if one considers the high asymmetry of this case, the similarity attained can be deemed satisfactory.

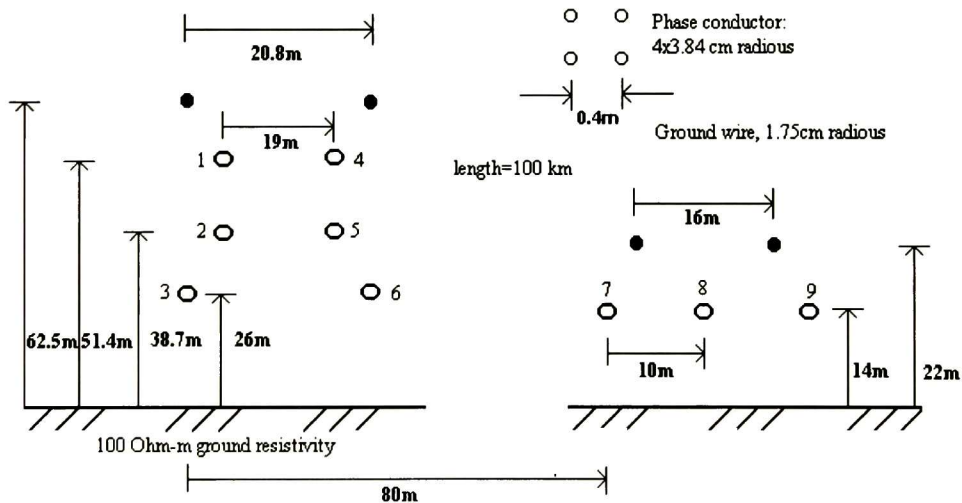


Fig. 3.4 Configuration for highly asymmetric overhead line

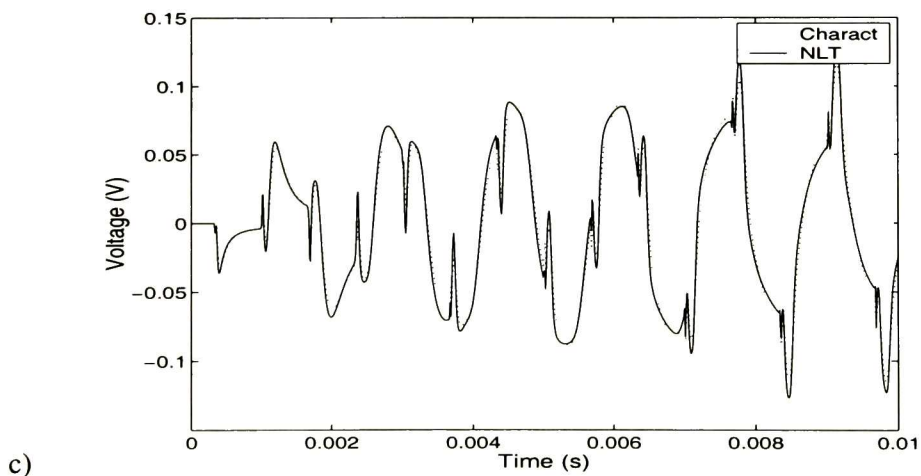
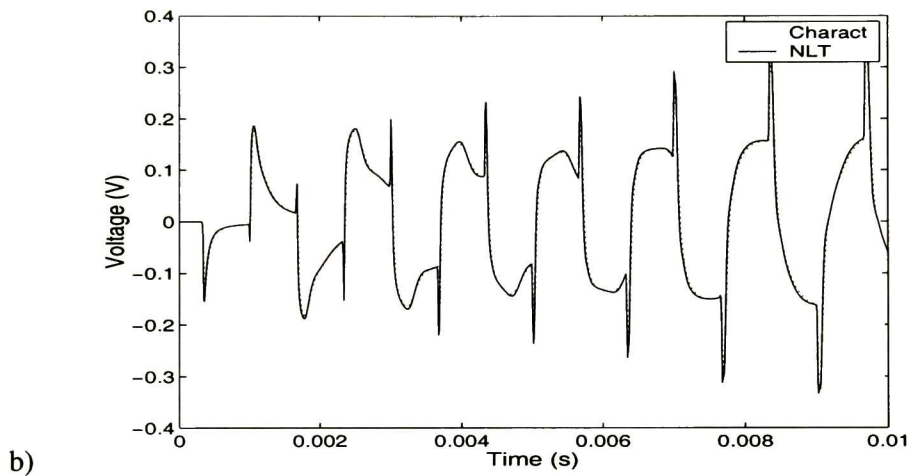
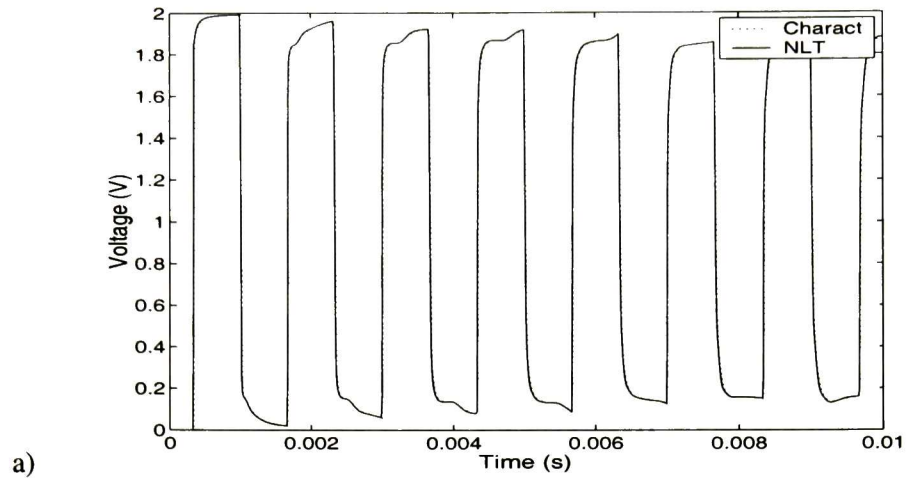


Fig. 3.5 Open circuit voltages at the receiving end for highly asymmetric overhead line

a) Conductor 1, b) Conductor 6, c) Conductor 9

C) Long underground cable system

Figure 3.6 provides the transversal geometry of an underground transmission system, along with the electrical properties of the earth, of its conducting and of its insulating layers. The system consists of three single core coaxial cables and is 10 km long. At the sending end, core conductor number 1 is to be excited with a voltage unit step while the other cores and sheaths are grounded. At the receiving end all the cores and the sheaths are open ended. Mention is made here as to the fact that this test case is adopted from [45]. Figures 3.7a-3.7b show the voltage waveforms at the receiving end for conductors 1, 3 and 6, respectively. All these results were obtained both, with the Characteristics model and with the NLT method. In all these cases, the differences are not noticeable by the eye. For the simulation with the method of Characteristics the line was divided in 16 sections of length $\Delta x = 625$ m.

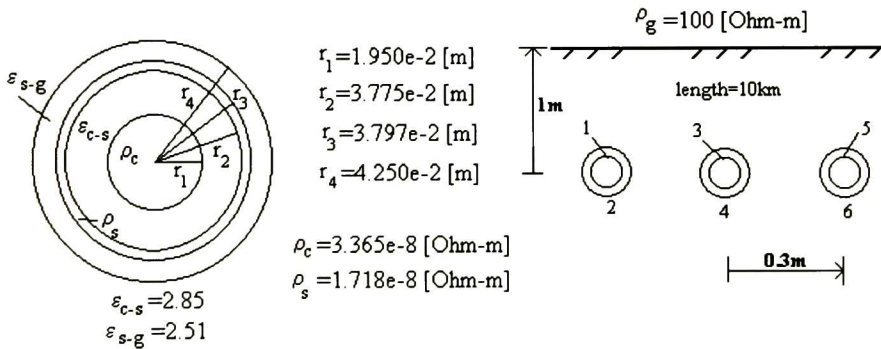


Fig. 3.6 Configuration for underground cable system

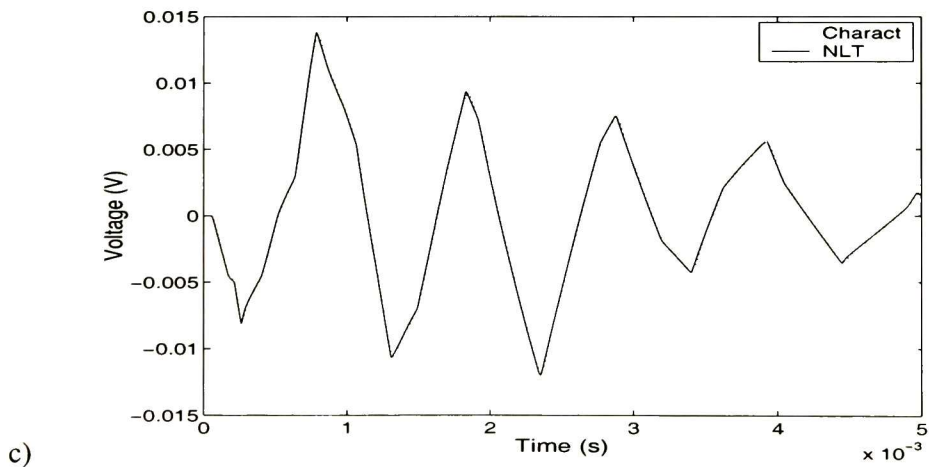
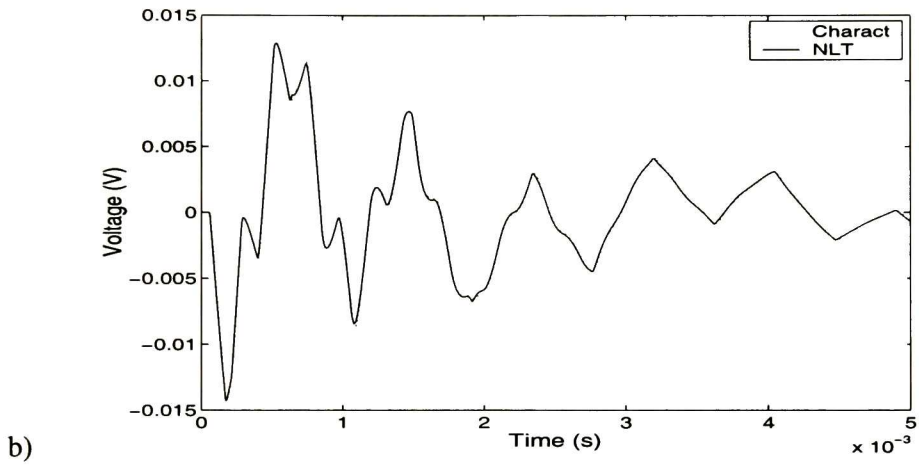
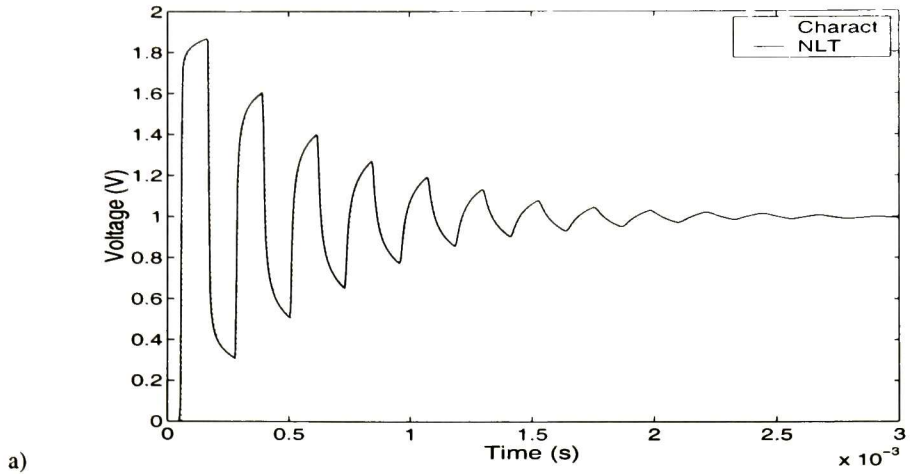


Fig. 3.7 Open circuit voltages at the receiving end for underground cable system
 a) core conductor 1, b) core conductor 3 and c) sheath conductor 6

3.6 Remarks

The multiconductor line model developed in [28], that is based on the method of Characteristics, has been extended here into a full frequency dependent line model. Other full frequency line models, based on traveling wave concepts have been recently developed [41, 43, 45]. Compared to these, the one of Characteristics one has two advantages. The first is that it only requires the identification and synthesis of one symmetric matrix; that is, the transient resistance matrix $\mathbf{R}'(s)$. The second is that it only requires one matrix-vector convolution per simulation time step. Traveling wave models, on the other hand, require the identification and synthesis of two matrices; namely, the characteristic admittance symmetric matrix $\mathbf{Y}_c = \sqrt{(\mathbf{YZ})^{-1}}\mathbf{Y}$ and the non-symmetric propagation matrix $\mathbf{H} = \exp(-\sqrt{\mathbf{YZ}l})$. The synthesis of the \mathbf{H} matrix further requires the identification of n modal delays. In addition to this, traveling wave models must perform three matrix-vector convolutions at each simulation time step.

The main advantage of traveling wave models perhaps is that they do not require spatial subdivisions for those cases of long homogeneous line sections. Therefore, the Characteristics line model is computationally more efficient, only for study cases in which lines have to be discretized. This is the case of the first application example provided here. Examples 2 and 3 show that, in spite of its lower numerical efficiency, the proposed model is applicable to cases of long homogeneous line sections providing a remarkable accuracy.

IV MODELING OF NON- UNIFORM TRANSMISSION LINES FOR TIME DOMAIN SIMULATION OF ELECTROMAGNETIC TRANSIENTS

4.1 Introduction

A few examples of non-uniform lines (NULs) in power systems are: overhead lines with sagging conductors, lines crossing rivers, lines entering substations and tall metallic structures struck by lightning. Most methods being proposed in the specialized literature deal with lossless, single-phase lines where a particular variation of the line parameters is assumed. A more general modeling methodology is therefore required.

In this chapter a more general methodology for NUL modeling is presented. Although the method of Characteristics used in the previous two chapters provides an adequate basis for this undertake, it was deemed that a change of approach was strategically advantageous. One strong reason is the availability of a frequency domain model for NULs developed by Semlyen which could be converted to time domain (TD) with a reasonable amount of effort. Another strong reason is that extending the method of Characteristics to multiconductor NUL is perhaps a PhD topic by itself. A third reason is that the frequency domain and TD methods will provide an invaluable support for this extension of the method of Characteristics.

The methodology of frequency domain synthesis and time domain recursive convolutions is thus adopted here. The result methodology can be applied to multiconductor lines with frequency dependent parameters. The models can also be used for representation of any geometrical configuration, such as towers. In addition, the models can be interfaced with the existing time domain programs, for instance the EMTP.

4.2 Terminal relations in frequency domain for NUL

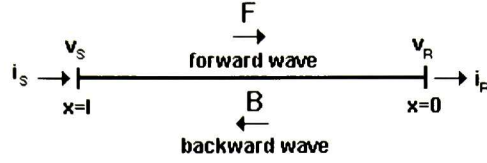


Fig. 4.1 Notation and reference directions for NUL

In the frequency domain, expression (4.1) represents the relation between voltages and currents at the two ends of the single-phase or the multiconductor line of Fig. 4.1 [38]:

$$\begin{bmatrix} v_S \\ i_S \end{bmatrix} = \begin{bmatrix} A & B \\ C & D \end{bmatrix} \begin{bmatrix} v_R \\ i_R \end{bmatrix} = \begin{bmatrix} W_{Fv} & W_{Bv} \\ W_{Fi} & W_{Bi} \end{bmatrix} \begin{bmatrix} \Lambda_F & \\ & \Lambda_B \end{bmatrix} \begin{bmatrix} W_{Fv} & W_{Bv} \\ W_{Fi} & W_{Bi} \end{bmatrix}^{-1} \begin{bmatrix} v_R \\ i_R \end{bmatrix} \quad (4.1)$$

where the $ABCD$ matrix defines the relation voltage/current between the two ends of the line and is numerically calculated by solving,

$$\frac{d}{dx} \begin{bmatrix} A(x) & B(x) \\ C(x) & D(x) \end{bmatrix} = \begin{bmatrix} 0 & Z(x) \\ Y(x) & 0 \end{bmatrix} \begin{bmatrix} A(x) & B(x) \\ C(x) & D(x) \end{bmatrix} \quad \begin{bmatrix} A(0) & B(0) \\ C(0) & D(0) \end{bmatrix} = I_{2n \times 2n} \quad (4.2)$$

In (4.2) I is the identity matrix, n is the number of phases and Z and Y are the impedance and the admittance matrices of the line calculated analytically or obtained from measurement. If Z and Y are calculated analytically, the $ABCD$ matrix is obtained by chain multiplication of matrices for line segments. In the present work the concept of complex depth is used to calculate parameters of lines and towers [12], [50].

Equation (4.1) contains the modal (eigenvalue/eigenvector) decomposition of the $ABCD$ matrix. This gives the following relation between the forward (F) and the backward (B) waves and the propagation functions Λ_F , Λ_B in the forward and the backward directions:

$$\begin{bmatrix} u_{F,S} \\ u_{B,S} \end{bmatrix} = \begin{bmatrix} \Lambda_F & \\ & \Lambda_B \end{bmatrix} \begin{bmatrix} u_{F,R} \\ u_{B,R} \end{bmatrix} \quad (4.3)$$

Equation (4.3) relates variables of the traveling wave formulation. The transformation to phase domain quantities, valid for both ends of the line, is given by

$$\begin{bmatrix} v \\ i \end{bmatrix} = \begin{bmatrix} W_{Fv} & W_{Bv} \\ W_{Fi} & W_{Bi} \end{bmatrix} \begin{bmatrix} u_F \\ u_B \end{bmatrix} \quad (4.4)$$

The relation between the forward and the backward propagation functions is

$$\Lambda_B = \Lambda_F^{-1} \quad (4.5)$$

The following inverse transformation matrix for (4.4) is defined:

$$\begin{bmatrix} W'_{Fv} & W'_{Fi} \\ W'_{Bv} & W'_{Bi} \end{bmatrix} = \begin{bmatrix} W_{Fv} & W_{Bv} \\ W_{Fi} & W_{Bi} \end{bmatrix}^{-1} \quad (4.6)$$

Definitions for the characteristic admittances in the forward and the backward directions for (4.4) are,

$$Y_{C,F} = W_{Fi} W_{Fv}^{-1} \quad (4.7a)$$

and

$$Y_{C,B} = W_{Bi} W_{Bv}^{-1} \quad (4.7b)$$

The backward propagation functions for the symmetrical line (Fig. 4.6), the river crossing line (Fig. 4.13) and the vertical structure (Fig. 4.9) applications presented in this chapter are shown in Figs. 4.2 to 4.5. Fig. 4.2 corresponds to the symmetrical line. Figs. 4.3 and 4.4 correspond to the river crossing line. Fig. 4.3 shows the impact of ground resistivity on the propagation function. The graphs of Fig. 4.4 are the same as those of Fig. 4.3a when plotted in a linear horizontal scale. Fig. 4.5 corresponds to the vertical structure line.

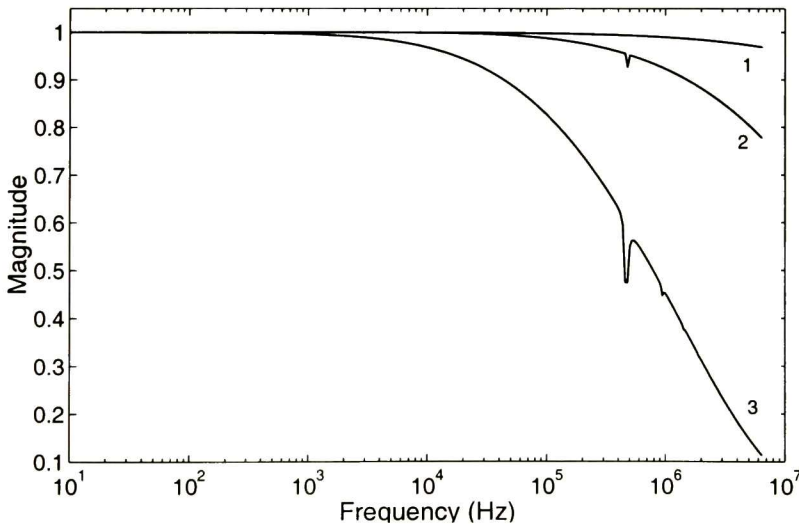


Fig. 4.2 Modal backward propagation functions for the three-phase symmetrical line of Fig. 4.6

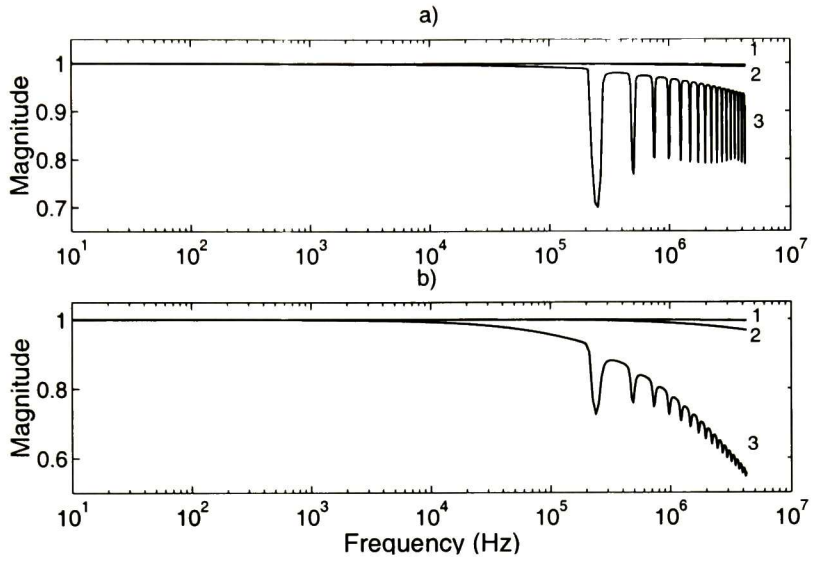


Fig. 4.3 Modal backward propagation functions for the three-phase river crossing. a) $\rho_t = 10 \Omega\text{-m}$, b) $\rho_t = 1000 \Omega\text{-m}$

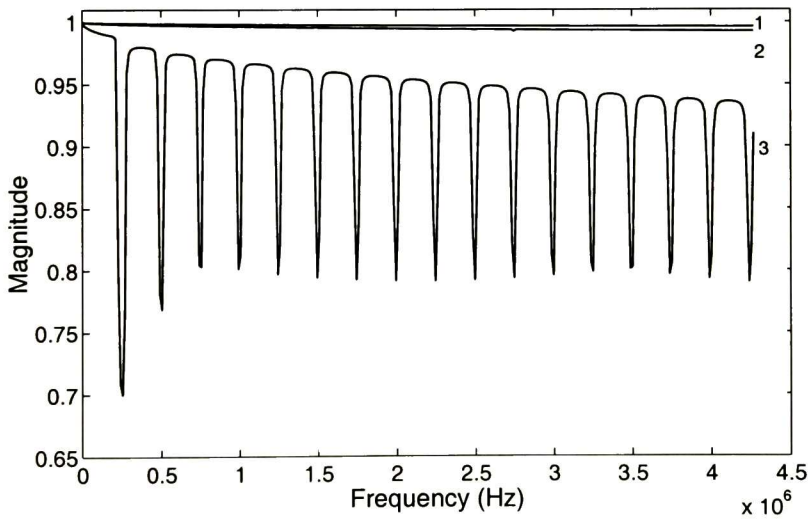


Fig. 4.4 Modal backward propagation functions for the three-phase river crossing $\rho_t = 10 \Omega\text{-m}$

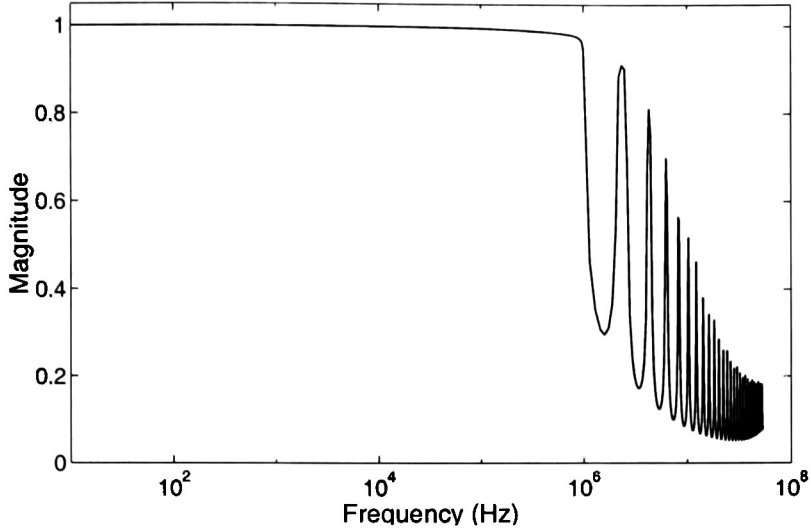


Fig. 4.5 Backward propagation function for the single-phase vertical structure

4.3 Time domain model for NUL

The following provides the derivation of the time domain model in the forward direction (see Fig. 4.1). An analogous procedure can also be applied for the backward direction.

Eliminating u_B from (4.4) and using (4.7b) yield:

$$Y_{C,B}v_R - i_R = (W_{Bi}W_{Bv}^{-1}W_{Fv} - W_{Fi})u_{F,R} \quad (4.8)$$

Substituting (4.3) into (4.8) gives

$$Y_{C,B}v_R - i_R = T_F \Lambda_B u_{F,S} \quad (4.9)$$

where

$$T_F = W_{Bi}W_{Bv}^{-1}W_{Fv} - W_{Fi} \quad (4.10)$$

and, from (4.4) and (4.6),

$$u_{F,S} = W'_{Fv}v_S + W'_{Fi}i_S \quad (4.11)$$

Thus, (4.9) represents the “Norton-type” relation between the receiving end voltages and currents needed in the calculation of transients. A next step is to approximate the parameters $Y_{C,B}$, T_F , Λ_B , W'_{Fv} , and W'_{Fi} , by rational functions and to use state-space realizations to solve (4.9) and (4.11) in the time domain [44]. For this solution, the corresponding expression for the terminal conditions of the line (node R in Fig. 4.1) must be taken into account together with numerical solution of the state-space approximations. As mentioned earlier, similar equations are derived for the backward direction and used for the sending end.

4.4 Applications

In this section, three applications of the model described above are presented. Also, comparisons with the results obtained from other methods are shown.

A) Symmetrical three-phase line

Fig. 4.6 shows the configuration of a flat three-phase NUL consisting of seven equal segments. Each segment at the length of 312.2 m and the maximum height of 26.2 m at the tower and the minimum height of 15.24 m at the mid-span. Each phase consists of one conductor with the radius of $r = 2.54$ cm. The ground resistivity is assumed to be $100 \Omega\text{-m}$. The configuration of the line in Fig. 4.6 is similar to the one used in [1] for measurements of voltage and current propagating along the line.

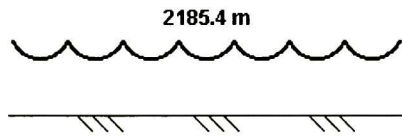


Fig. 4.6 Symmetrical, flat, three-phase NUL

Three identical voltage waveforms reported in [1] are simultaneously injected in all phases at the sending end when the receiving end is open. The sending end voltage and the corresponding receiving end voltage are shown in Fig. 4.7, which illustrates both the experimental [1] and the simulation results. The simulation result is obtained based on the proposed time domain (TD) model. In addition to the comparison with the experimental results [1], the TD model is also validated by comparing the result with those obtained from a frequency domain methodology using the Numerical Laplace Transform (NLT) [17], Fig. 4.8a. In the comparison with NLT, a voltage wave $v(t) = K(e^{-t/t_0} - e^{-t/t_1})$ is applied using the same terminal conditions as in the preceding case, with $K = -1.0017$ V, $t_0 = 0.205 \mu\text{s}$ and $t_1 = 1182 \mu\text{s}$. Figs. 4.7 and 4.8a demonstrate that the results obtained from the TD model closely agree with the measurement results and are almost identical to those obtained from the NLT approach. The reason for the fluctuation in the voltage waveform is discussed in Section 4.5.

In Fig. 4.8a the results obtained with the proposed TD approach and the NLT method are compared with those obtained with the method of Characteristics. Fig. 4.8a shows that there exists a significant difference between the traces obtained with full representation of frequency dependence, *i.e.* NLT and TD, and the one with frequency independent parameters using the method of Characteristics [46]. Fig. 4.8a shows that the representation of the frequency dependence of the line parameters is important in the case of not very short NULs. When the line is simulated with frequency dependent and uniform parameters, the resulting curve is close to the experimental one, only the wave crest ripple is not reproduced. This is shown in Fig. 4.8b.

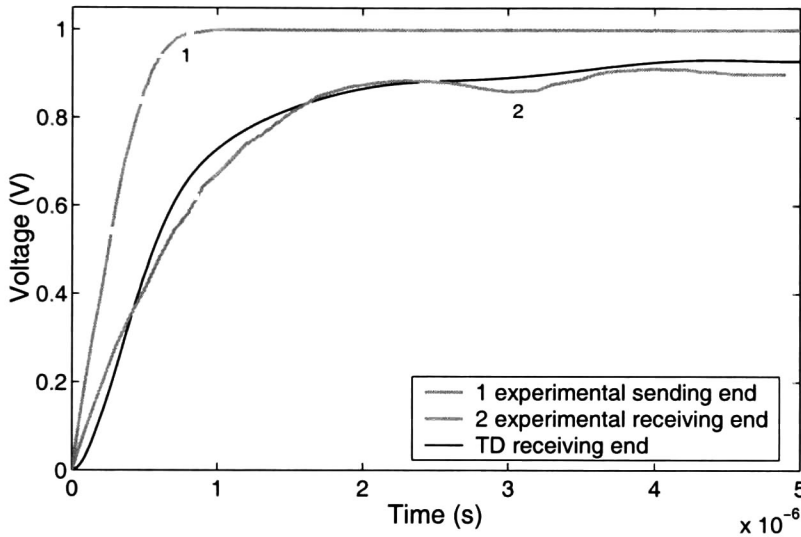


Fig. 4.7 Time domain simulation and experimental results for the line of Fig. 4.6

B) Vertical structure

The vertical structure, Fig. 4.9, examined in this example is the one introduced in [14]. The structure is used to represent a tower. It has a circular cross-section with radius of 0.7 m. In this application the equations given in [50] are used to calculate the characteristic impedance. The selected radius results in a value for the characteristic impedance at the top of the tower equal to that obtained from $Z_c = 50 + 35\sqrt{x}$ used in [14], [30], [38]. The ground resistivity is assumed to be 30 Ω -m.

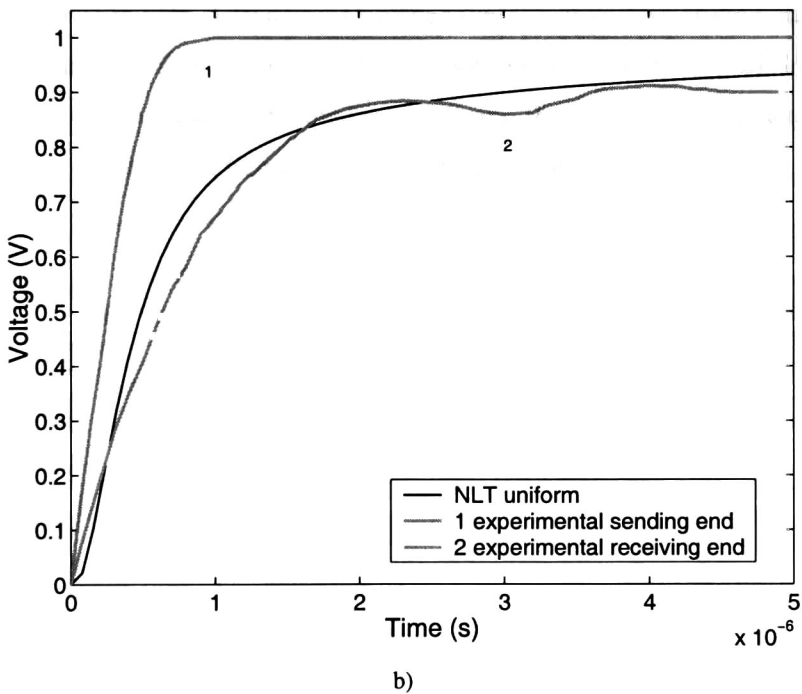
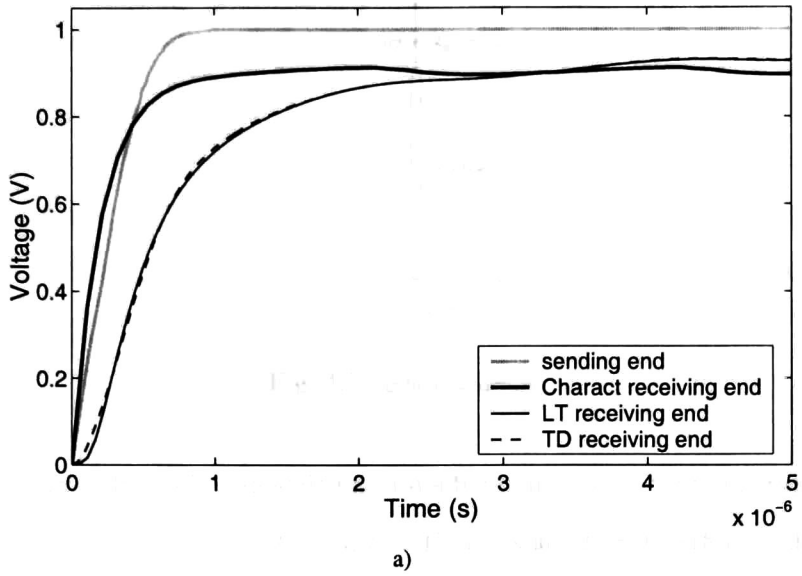


Fig. 4.8 Simulations for the line of Fig. 4.6

a) Characteristics, TD and NLT, b) NLT without considering non-uniform effects

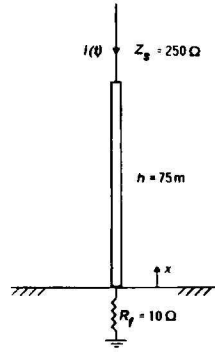


Fig. 4.9 Vertical structure

The lightning stroke in Fig. 4.9 is modeled as a double-exponential Norton current source given by $i(t) = K(e^{-t/t_0} - e^{-t/t_1})$ with $K = 62\text{ kA}$, $t_0 = 17.63\ \mu\text{s}$ and $t_1 = 0.0316\ \mu\text{s}$ [30], [38]. A more advanced model of the lightning stroke is given in [47]. The voltage and the current at the top of the structure are shown in Figs. 4.10 and 4.11 respectively. The voltage at the bottom is shown in Fig. 4.12. The results from Figs. 4.10 to 4.12 agree with those reported in [30]. In contrast to the longer NUL of Fig. 4.8, the results obtained with TD and the method of Characteristics are very close. This is due to the fact that frequency dependence in the case of short lines does not have a significant effect.

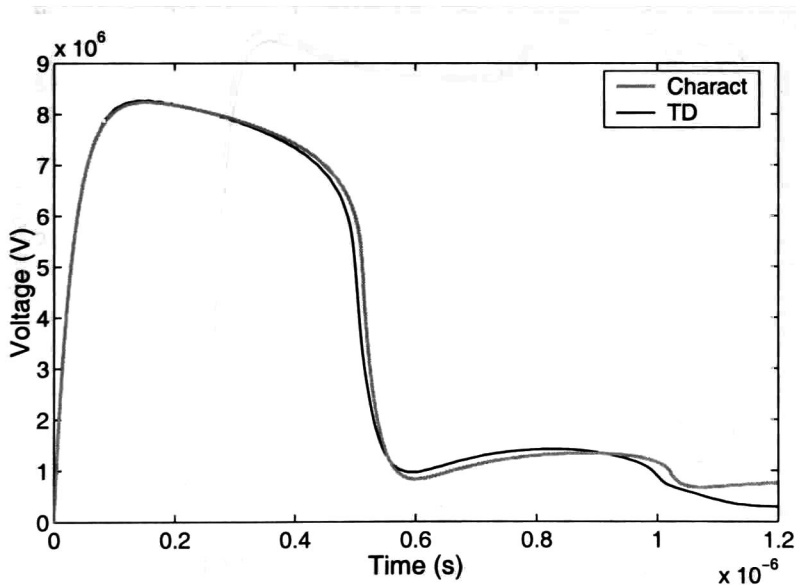


Fig. 4.10 Voltage at the top of vertical structure

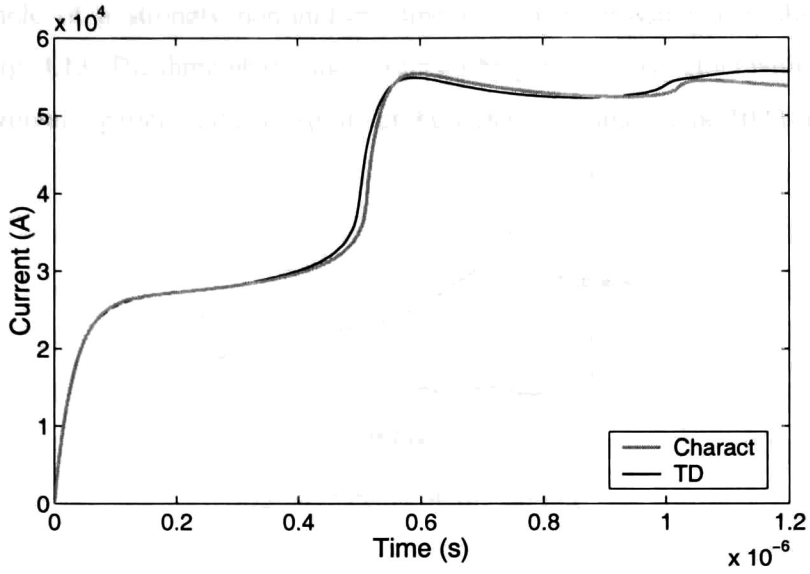


Fig. 4.11 Current at the top of vertical structure

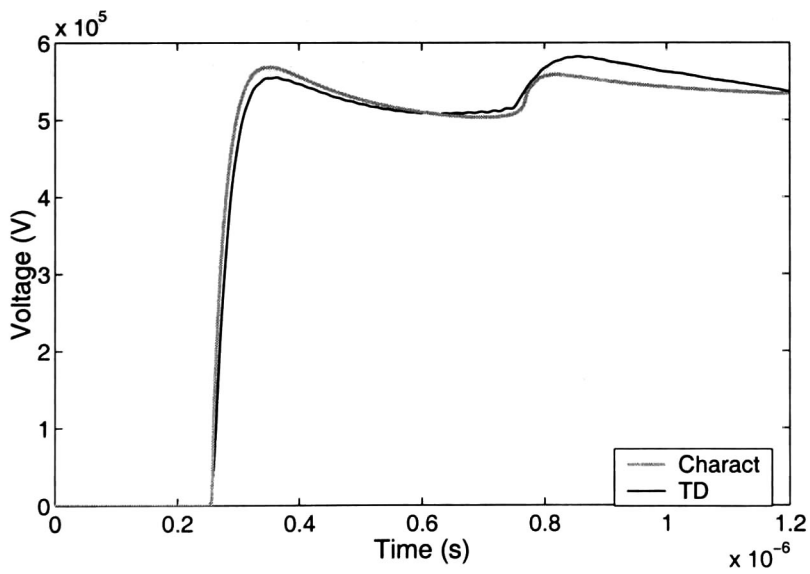


Fig. 4.12 Voltage at the bottom of vertical structure

C) River crossing

Another example of a strongly non-uniform line is a river crossing, e.g. the configuration presented in Fig. 4.13. The three-phase line is formed by parallel conductors with 2.54 cm radius and 10 m horizontal separation; the resistivity of the water is assumed to be $10 \Omega\text{-m}$.

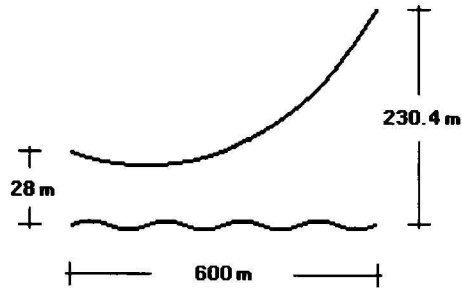


Fig. 4.13 Profile of river crossing

The sending end is at the elevation of 28 m. A unit step voltage is applied to the conductors at the sending end when the receiving end is open. The voltage waveform resulting from the simulation based on the TD method is presented in Fig. 4.14. Fig. 4.14 also shows the results obtained based on the NLT method. Fig. 4.14 shows that the TD method presents oscillations in the waveform resulting from the simulation. The frequency of these oscillations is closely related with the maximum frequency, f_{max} , used to calculate the line parameters. Further explanation regarding the oscillations is given in Section 4.5.

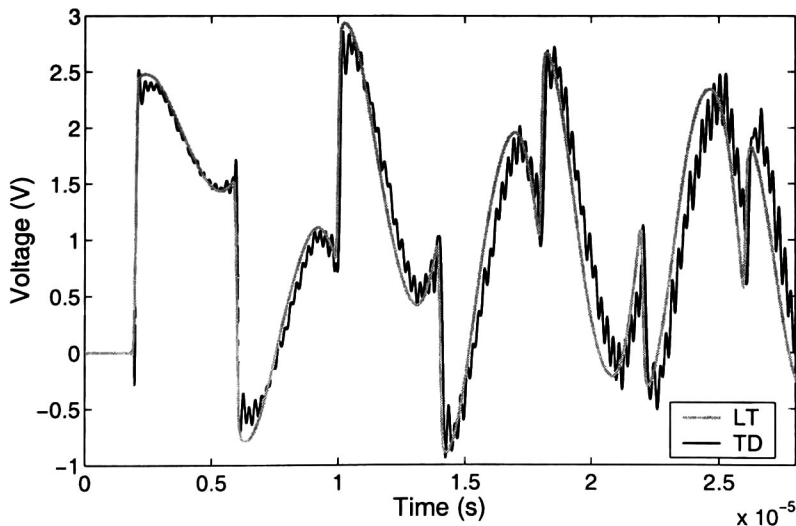


Fig. 4.14 Voltage at the receiving end phases 1 and 3 for the line of Fig. 4.13

4.5 Discussion of results

Figure 4.2 shows that modal backward propagation functions 1 and 2 present a spike at the fundamental frequency $f_o = c/2l$ related to the length of the line l , and the light velocity c . Further analysis of data corresponding to this figure shows that the three functions present thus spikes at frequencies harmonically related to f_o .

These spikes translate into superimposed small fluctuations in time domain as can be seen in the results presented in Figs. 4.7 and 4.8 for the symmetrical line of Fig. 4.6. In this application $f_o \cong 480.46$ kHz corresponding to the frequency of fluctuations shown in Figs. 4.7 and 4.8. Fig. 4.2 shows that only the first spike is of considerable magnitude.

Fig. 4.3 shows the propagation function for the river crossing line of Fig. 4.13. Increasing non-uniformity by asymmetry results in larger magnitudes of the spikes (as compared to those of Fig. 4.2) as shown in Fig. 4.3. An analogous remark is that a smaller ground resistivity increases the magnitudes of the spikes (see Fig. 4.3).

To compute transients in time domain, the range of frequencies must be finite. Frequency truncation can introduce spurious oscillations or even instability in the time domain simulations when the spikes, in frequencies higher than f_{max} , are of considerable magnitude. This phenomenon represents Gibbs oscillations that can be diminished in a frequency domain program, *e.g.* NLT, by using windows to smooth the effect of truncation. In this thesis the trapezoidal rule (TR) is initially used to discretize the state-space realizations mentioned above. However, depending on the non-uniformity and ground resistivity, the backward Euler method (BE) is used to act as a filter in time domain simulations instead of TR to eliminate the spurious oscillations like those shown in Fig. 4.14. Using BE effectively damps out the natural oscillations due to the frequency truncation as described in Appendix A. Using the above feature, the simulation for the river crossing line is repeated by using BE and the results are shown in Fig. 4.15 in which the spurious oscillations (Fig. 4.14) are not present in the TD results.

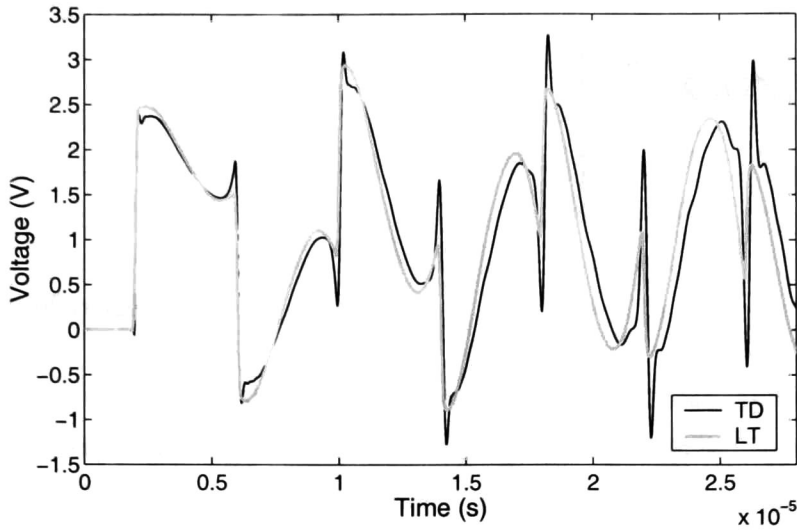


Fig. 4.15 Voltage at the receiving end phases 1 and 3 for the line of Fig. 4.13 using BE

4.6 Remarks

The topic of NULs started receiving due attention recently. Criteria for including NUL effects, as well as for combining these with the frequency dependent ones, are not ready yet. This chapter introduces and develops a time domain methodology to compute electromagnetic transients in single-phase and multiconductor NULs including frequency dependent effects. The term NUL encompasses line geometries where the line parameters have longitudinal variations, *e.g.* lines crossing rivers, lines entering substations, and vertical tower structures. The proposed formulation is based on the concept of travelling waves and takes into account the frequency dependence of the line parameters. The model is used to compute electromagnetic transients for three different non-uniform geometries and its accuracy is demonstrated by comparing the results with those obtained from the method of Characteristics and measurement results reported by other investigators. A salient feature of the methodology is that it can be readily included in time domain simulation packages, *e. g.* the EMTP.

5.1 Summary of results

This thesis deals with advanced modeling techniques for transmission lines. Although the focus is on power lines, it is suggested that the techniques developed here are applicable to electronic and communication line problems. The line analysis problem has been attacked from two complementary approaches. The first is a time domain based one which uses the theory of Characteristics of PDEs. The second is a frequency domain based which produces a time domain model.

An existing Characteristics based model for single-phase lines with corona, developed in [32], has been extended to include frequency dependence (or linear dispersion) effects. The resulting model has provided simulations closer to experiments than others proposed elsewhere. Since the method of Characteristics eliminates numerical oscillations, the new model is able to handle multipeak waveforms and multiple reflections [33].

The above mentioned method of Characteristics has also been extended for handling multiconductor lines with frequency dependent parameters and excited by a distributed source. The resulting model requires to synthesize only one matrix function compared with two required by traveling wave based models. This has the advantage that the number of convolutions is decreased substantially. It has been shown through an application example that the new model is more accurate and convenient than the standard way of dealing with illuminated lines consisting in the use of EMTP J. Martí's line model [34]. For cases of long homogeneous lines that do not require spatial subdivision, the new model is computationally less efficient than traveling wave models; nevertheless, the model synthesis still is simpler and the attained results are remarkably accurate. The new model has been benchmarked against the NLT method in two applications that might be considered pathological. One involves a long and highly asymmetrical overhead line. The other consists in a long underground cable. The new model requires line subdivisions; the

required subsection lengths have resulted surprisingly longer than expected, in the order of $\Delta x = 625\text{-}2857$ m. This range should be compared with the ones required by an akin model, the Z-cable model [51], where $\Delta x = 100$ m is a typical figure.

As for the case of non-uniform multiconductor lines including frequency dependent effects, the method of Characteristics is adequate. However, it has been deemed more convenient to attack this problem first from another complementary angle. A frequency domain model previously developed by Semlyen and published as a discussion to [38], has been adopted here as basis for the synthesis of a time domain model for such lines. This model, like the one based on Characteristics, has the added advantage of permitting its direct incorporation into the EMTP. The TD model here proposed constitutes a valuable tool for both, the further development of a Characteristics based NUL model and the establishment of guidelines to include non-uniform effects in line analysis.

5.2 Recommendations for further developments

The following is a list of projects recommended as continuation of the work reported in this thesis.

1) Multiconductor lines with corona and skin effects.

Most of the existing models for multiconductor lines with corona are based on standard linear modal analysis; however, corona is a non-linear phenomenon. The theory of Characteristics permits dealing with multiconductor lines affected by corona in a mathematically rigorous manner. This topic might well be by itself a Ph. D. project. An additional development is the inclusion of frequency dependent effects.

2) Analysis of multitransposed lines.

The multiconductor model of chapter 3, for dealing with distributed sources, can be adopted for analyzing multitransposed lines and cables. In these applications, the resulting adaptation seems to offer more accuracy and numerical efficiency than traveling wave models.

3) Non-uniform multiconductor line model.

To develop a model based on Characteristics that be able handle non-uniform multiconductor lines. Such a model would be a highly convenient complement of the model proposed in chapter 4. These two models would be valuable for providing a better understanding of NULs.

REFERENCES

- [1] **C. F. Wagner, I. W. Gross, B. L. Lloyd**, “*High-Voltage Impulse Test on Transmission Lines*”, AIEE Trans., vol. 73, pt. III-A, pp. 196-210, April 1954.
- [2] **C. F. Wagner, B. L. Lloyd**, “*Effects of Corona on Traveling Waves*”, AIEE Trans., pp. 858-872, June 1955.
- [3] **M. E. Van Valkenburg**, “*Introduction to Modern Network Synthesis*”, John Wiley & Sons, Inc., 1960.
- [4] **L. M. Wedepohl**, “*Application of Matrix Methods to the Solution of Travelling Wave Phenomena in Polyphase Systems*”, Proc. IEE, vol. 110, no. 12, pp. 2200-2212, December 1963.
- [5] **C. D. Taylor, R. S. Satterwhite, C. W. Harrison**, “*The Response of a Terminated Two-Wire Transmission Line Excited by a Nonuniform Electromagnetic Field*”, IEEE Trans. on Antenna and Propagation, vol. AP-13, 1965.
- [6] **E. M. Stafford, D. J. Evans and N. G. Hingorani**, “*Calculation of Travelling Waves on Transmission Systems by Finite Differences*”, Proc. IEE, vol. 112, no. 5, pp. 941-948, May 1965.
- [7] **A. Budner**, “*Introduction of Frequency Dependent Line Parameters into an Electromagnetic Transients Program*”. IEEE Trans. Power Apparatus and Systems, vol. PAS-89, pp. 88-97, January 1970.
- [8] **J. K. Snelson**, “*Propagation of Travelling Waves on Transmission Lines-Frequency Dependent Parameters*”, IEEE Trans. Power Apparatus and Systems, vol. PAS-91, pp. 85-91, January/February 1972.
- [9] **G. B. Whitham**, “*Linear and Nonlinear Waves*”, John Wiley & Sons, U. S. A. 1974.
- [10] **A. Semlyen, A. Dabuleanu**, “*Fast and Accurate Switching Transient Calculations on Transmission Lines with Ground Return Using Recursive Convolutions*” IEEE Trans. Power Apparatus and Systems, vol. PAS-94, pp. 561-571, March/April 1975.
- [11] **R. Radulet, Al. Timotin, A. Tugulea, A. Nica**, “*The Transient Response of the Electric lines Based on the Equations with Transient Line-Parameters*”, Rev. Roum. Sci. Techn., vol. 23, no. 1, pp. 3-19, 1978.

- [12] **A. Deri, G. Tevan, A. Semlyen, and A. Castanheira**, “*The Complex Ground Return Plane: A Simplified Model for Homogeneous and Multi-layer Earth Return*”, IEEE Trans. Power Apparatus and Systems, vol. PAS-100, no. 8, pp. 3686-3693, August 1981.
- [13] **J. R. Martí**, “*Accurate Modelling of Frequency-Dependent Transmission Lines in Electromagnetic Transient Simulations*”, IEEE Trans. Power Apparatus and Systems, vol. PAS-101, no. 1, pp. 147-157, January 1982.
- [14] **C. Menemenlis and Z. T. Chun**, “*Wave Propagation on Nonuniform Lines*”, IEEE Trans. Power Apparatus and Systems, vol. PAS-101, no. 4, pp. 833-839, April 1982.
- [15] **L.M. Wedepohl**, “*Theory of Natural Modes in Multiconductor Transmission Lines*” Lecture Notes for Course ELEC-552, The University of British Columbia, 1982.
- [16] **C. Gary, A. Timotin, D. Cristescu**, “*Prediction of Surge Propagation Influenced by Corona and Skin Effect*”, IEE Proc., vol. 130, no. 5, pp. 264-272, July 1983.
- [17] **L.M. Wedepohl**, “*Power System Transients: Errors Incurred in the Numerical Inversion of the Laplace Transform*” Proc. of the Twenty-Sixth Midwest Symposium on Circuits and Systems, pp. 174-178, August 1983.
- [18] **A. Semlyen, Huang Wei-Gang**, “*Corona Modelling for the Calculation of Transients on Transmission Lines*”, IEEE Trans. on Power Delivery, vol. PWRD-1, no. 3, pp. 228-239, July 1986.
- [19] **H. W. Dommel**, “*Electromagnetic Transients Program Reference Manual (EMTP Theory Book)*”, Prepared for Bonneville Power Administration, P. O. Box 3621, Portland, Oregon 97208, U.S.A., 1986.
- [20] **M. Abdel-Salam, E. Keith Stanek**, “*Mathematical-Physical Model of Corona from Surges on High-Voltage Lines*”, IEEE Trans. on Industry Applications, vol. IA-23, no. 3, pp. 481-489, May/June 1987.
- [21] **L. Martí**, “*Simulation of Transients in Underground Cables with Frequency-Dependent Modal Transformation Matrices*”, IEEE Trans. on Power Delivery, vol. 3, no. 3, pp. 1099-1110, July 1988.
- [22] **R. E. Skelton**, “*Dynamic System Control: Linear System Analysis and Synthesis*” Ed. John Wiley and Sons, U. S. A., 1988.
- [23] **C. Gary, D. Cristescu, G. Dragan**, “*Distorsion and Attenuation of Travelling Waves Caused by Transient Corona*”. CIGRE Report, Study Committee 33: Overvoltages and Insulation Coordination, 1989.
- [24] **J. R. Marti and J. Lin**, “*Suppression of Numerical Oscillations in the EMTP*”, IEEE Trans. Power Systems, vol. 4, no. 2, pp. 739-747, May 1989.

- [25] **S. Carneiro, J. R. Martí**, “*Evaluation of Corona and Line Models in Electromagnetic Transient Simulations*”, IEEE Trans. on Power Delivery, vol. 6, no. 1, pp. 334-341, January 1991.
- [26] **M. Ishii, T. Kawamura, T. Kouno, E. Ohsaki, K. Murotani, and T. Higuchi**, “*Multistory Transmission Tower Model for Lightning Surge Analysis*”, IEEE Trans. Power Delivery, vol. 6, no. 3, pp. 1327-1335, July 1991.
- [27] **W. F. Ames**, “*Numerical Methods for Partial Differential Equations*”, Academic Press Inc, Third Ed., USA, 1992.
- [28] **J. L. Naredo, P. Moreno, A. Soudack and J. R. Martí**, “*Frequency Independent Representation of Transmission Lines for Transient Analysis Through the Method of Characteristics*”, Proc. of The Athens Power Tech. 1993, NTUA IEEE/PES Joint International Power Conference 1993, Athens, Greece, vol. 1, pp. 28-32, September 5-8 1993.
- [29] **S. Carneiro, H. W. Dommel, J. R. Martí, H. M. Barros**, “*An Efficient Procedure for the Implementation of Corona Models in Electromagnetic Transients Programs*”. Paper 93SM 401-0 PWRD, IEEE Trans. on Power Delivery, vol. 9, no. 4, April 1994.
- [30] **E. A. Oufi, A. S. Alfuhaid, and M. M. Saied**, “*Transient Analysis of Lossless Single-phase Nonuniform Transmission Lines*”, IEEE Trans. Power Delivery, vol. 9, no. 3, pp. 1694-1700, July 1994.
- [31] **L. Silveira, M. Elfadel, J. White, M. Chilukuri and K. Kundert**, “*Efficient Frequency-Domain Modeling and Circuit Simulation of Transmission Lines*”, IEEE Trans. on Components, Packaging and Manufacturing Technology-Part B, vol. 17, no. 4, pp. 505-513, November 1994.
- [32] **J.L. Naredo, A.C. Soudack, J.R. Martí**, “*Simulation of Transients on Transmission Lines with Corona via the Method of Characteristics*”, IEE Proc. Gener. Transm. Distrib., vol. 142, no.1, pp. 81-87, January 1995.
- [33] **J. L. Naredo, P. Moreno Villalobos, A. C. Soudack, J. R. Martí**, “*Travelling Waves on Single Phase Lines Including Corona and Reflection Effects*”, ISHV-95 Conference Record, Subject 6, Paper 6789, Graz, Austria, August/September 1995.
- [34] **A. Xémard, Ph. Baraton and F. Boutet**, “*Modelling with EMTP of Overhead Lines Illuminated by an External Electromagnetic Field*”. Proc. of the International Conference on Power Systems Transients, pp. 39-44, Lisbon, Portugal, September 1995.
- [35] **F. Castellanos and J. R. Martí**, “*Phase Domain Multiphase Transmission Line Models*”, Proc. of the International Conference on Power Systems Transients, pp. 17-22, Lisbon, Portugal, September 1995.
- [36] **T. Noda, N. Nagaoka and A. Ametani**, “*Phase Domain Modeling of Frequency-Dependent Transmission Lines by Means of an ARMA Model*”, IEEE Trans. on Power Delivery, vol. 11, no. 1, pp. 401-411, January 1996.

- [37] **D. B. Kuznetsov and J. E. Schutt-Ainé**, “*Optimal Transient Simulation of Transmission Lines*”. IEEE Trans. on Circuits and Systems-I: Fundamental Theory and Applications, vol. 43, no. 2, pp. 110-121, February 1996.
- [38] **M. T. Correia de Barros, M. E. Almeida**, “*Computation of Electromagnetic Transients on Nonuniform Transmission Lines*” IEEE Trans. Power Delivery, vol. 11, no. 2, pp. 1082-1091, April 1996.
- [39] **F. J. Marcano**, “*Modeling of Transmission Lines Using Idempotent Decomposition*”, MAsc. Thesis, Department of Electrical Engineering, The University of British Columbia, Vancouver, Canada, August 1996.
- [40] **H. V. Nguyen, H. W. Dommel, and J. R. Martí**, “*Modelling of Single-phase Nonuniform Transmission Lines in Electromagnetic Transient Simulations*”, IEEE Trans. Power Delivery, vol. 12, no. 2, pp. 916-921, April 1997.
- [41] **F. Castellanos and J. R. Martí**, “*Full Frequency-Dependent Phase-Domain Transmission Line Model*”, IEEE Trans. on Power Systems, vol. 12, no. 3, pp. 1331-1339, August 1997.
- [42] **H. V. Nguyen, H. W. Dommel and J. R. Martí**, “*Direct Phase-Domain Modelling of Frequency-Dependent Overhead Transmission Lines*” IEEE Trans. on Power Delivery, vol. 12, no. 3, pp. 1335-1342, July 1997.
- [43] **F. J. Marcano and J. R. Martí**, “*Idempotent Line Model: Case Studies*”, Proc. of the International Conference on Power Systems Transients, pp. ,Seattle, Washington, June 1997.
- [44] **B. Gustavsen and A. Semlyen**, “*Combined Phase Domain and Modal Domain Calculation of Transmission Line Transients Based on Vector Fitting*”, IEEE Trans. Power Delivery, vol. 13, no. 2, pp. 596-604, April 1998
- [45] **A. Morched, B. Gustavsen and M. Tartibi**, “*A Universal Model for Accurate Calculation of Electromagnetic Transients on Overhead Lines and Underground Cables*”, IEEE Trans. on Power Delivery, vol. 14, no. 3, pp. 1032-1037, July 1999.
- [46] **J. A. Gutierrez, J. L. Naredo, L. Guardado, and P. Moreno**, “*Transient Analysis of Nonuniform Transmission Lines through the Method of Characteristics*”, Proc. of the ISH-99, 11th International Symposium on High Voltage Engineering, vol. 2, topic B, London, U. K., August 23-27, 1999.
- [47] **V. Shostak, W. Janischewskyj, and A. M. Hussein**, “*Expanding the Modified Transmission Line Model to Account for Reflections within the Continuously Growing Lightning Return Stroke Channel*” IEEE Power Engineering Society Summer Meeting 2000, vol. 4, pp. 2589-2602.

- [48] **C. A. Nucci, S. Guerrieri, M. T. Correia de Barros and F. Rachidi**, “*Influence of Corona on the Voltajes Induced by Nearby Lightning on Overhead Distribution Lines*”, IEEE Trans. on Power Delivery, vol. 15, no. 4, pp. 1265-1273, October 2000.
- [49] **M. S. Mamis and M. Koksal**, “*Lightning Surge Analysis using Nonuniform, Single-phase Line Model*”, IEE Proc. Gener. Transm. Distrib., vol. 148, no. 1, pp. 85-90, January 2001.
- [50] **J. A. Gutierrez, P. Moreno, J. L. Naredo, and L. Guardado**, “*Non Uniform Line Tower Model for Transient Studies*”, Proc. of the International Conference on Power Systems Transients, pp. 535-540, Rio de Janeiro, Brazil, June 2001.
- [51] **T. C. Yu and J. R. Martí**, “*zCable Model for Frequency Dependent Modelling of Cable Transmission Systems*”. Proc. of the International Conference on Power Systems Transients, pp. 55-60, Rio de Janeiro, Brazil, June 2001.

APPENDIX A

Damping Properties of Backward Euler Integration Rule

The damping effect of the Backward Euler (BE) method is described in [24]. Here a simple example is shown for illustration. Consider the homogeneous ODE with the natural frequency ω

$$\dot{x} = j\omega x \quad (\text{A.1})$$

and its analytical solution (with initial value $x = 1$)

$$x = e^{j\omega t} \quad (\text{A.2})$$

The solution given by (A.2) represents a circle in the complex plane and corresponds to an undamped solution in the time domain. Applying BE to (A.1) results in the following expression:

$$x - x^{old} = j\omega h x \quad (\text{A.3})$$

where h is the time step. The following continuous solution is assumed for the recursion (A.3):

$$x = e^{st} \quad (\text{A.4})$$

Substituting (A.4) in (A.3), such that $x^{old} = e^{s(t-h)}$, the parameter s is obtained as:

$$s = -\log(1 - j\omega h) / h \quad (\text{A.5})$$

Similarly, using trapezoidal integration method (TR) to solve (A.1), the parameter s becomes:

$$s = -\frac{1}{h} \log\left(\frac{1 - j\omega h / 2}{1 + j\omega h / 2}\right) \quad (\text{A.6})$$

The analytical solution in the time domain is compared with those obtained from BE and TR in Fig. A.1 taking 1.5 periods and using $N = 5$ and $N = 15$ steps per period. In Fig. A.1, the discrete solution of (A.2) is presented by points corresponding to N steps and the continuous solution joining these discrete points is added for clarity.

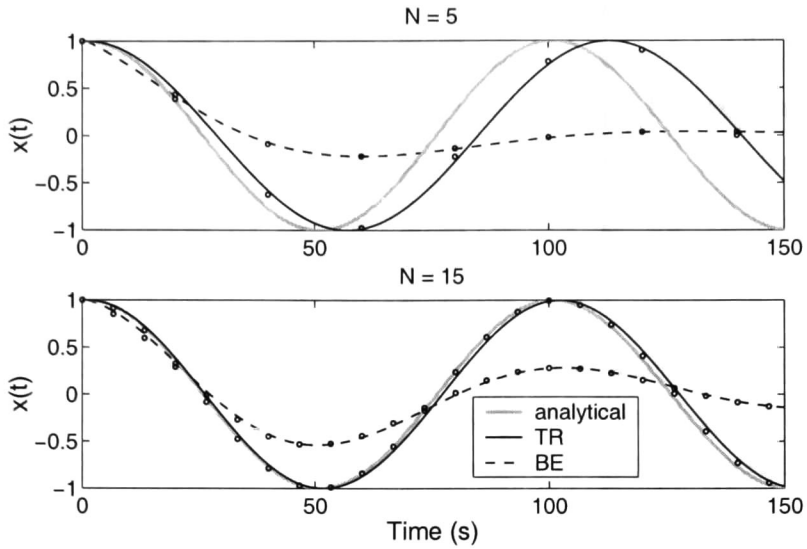


Fig. A.1 Example for damping, time domain

Fig. A.1 shows that the damping introduced by BE is significant even when a larger number of time steps is used. TR has no damping effect in terms of the magnitude of oscillations and the discretization error is visible only in the frequency of the oscillations.

Introducción

La confiabilidad de los sistemas de transmisión de energía eléctrica depende en gran medida de la precisión de los métodos de el análisis y diseño de los elementos que lo conforman. Las líneas y los cables de transmisión son elementos muy importantes de dichos sistemas. Esta tesis, por tanto, se aboca al desarrollo de modelos que permitan simular o reproducir el comportamiento transitorio de las líneas y los cables.

Los primeros modelos se basaron en el caso de líneas sin pérdidas, para las cuales sus ecuaciones descriptivas corresponden a la ecuación clásica de onda. La solución de D'Alembert a esta última, en términos de ondas viajeras, es bien conocida y constituye la base para el método de Bergeron y el modelo circuital tipo Norton para una línea ideal. En los últimos 30 años se han dedicado esfuerzos considerables para extender este modelo básico al caso de líneas multiconductoras que incluya pérdidas. Recientemente se ha desarrollado un modelo de línea basado en la teoría de matrices idempotentes [15]. Este modelo, a veces denominado "universal" [45], prácticamente resuelve el problema del modelado de líneas que sean multiconductoras, lineales, homogéneas y excitadas por fuentes concentradas.

Existen muchos casos en la práctica en que se requiere efectuar la subdivisión de una línea (o cable) para su análisis; entre ellos: 1) cuando la línea es no uniforme, 2) cuando es no lineal, como con la ocurrencia de efecto Corona, 3) cuando está excitada por una fuente distribuida debida a un campo electromagnético radiado y 4) cuando una línea homogénea tiene transposiciones múltiples y muy cercanas. Ejemplo de este último son los cables subterráneos con transposición de pantallas (cross-bonded). En todos estos casos, un modelo de línea basado en diferencias finitas puede ser más ventajoso que los usuales basados en ondas viajeras.

En esta tesis se reporta la construcción de tres modelos de línea. El primero que permite simular transitorios en líneas monofásicas considerando efectos Skin y Corona; es decir, con dispersiones lineal y no lineal. El segundo modelo permite simular líneas polifásicas considerando parámetros dependientes de la frecuencia y excitaciones por medio de fuentes distribuidas. El tercer modelo permite analizar transitorios en líneas polifásicas con parámetros dependientes de la frecuencia así como de la distancia; o sea, líneas no uniformes.

Líneas monofásicas con efectos corona y dependencia frecuencial

Por una parte el efecto Skin, tanto en el plano de tierra como en los conductores, provoca el fenómeno de dispersión lineal en una línea de transmisión. Por otra, el efecto Corona produce dispersión no lineal. Cuando el fenómeno Corona ocurre, el parámetro capacitancia de línea se convierte en una función de la tensión (o voltaje), y esto produce características no lineales en la propagación. Por tanto, los métodos del dominio del tiempo son considerados los más adecuados para analizar líneas con Corona; además, se debe recurrir a la discretización espacial de las líneas bajo estudio.

Un problema comúnmente encontrado en la solución numérica de las ecuaciones diferenciales parciales (EDPs) no lineales que describen a una línea es el de la aparición de oscilaciones artificiales [2]. Este problema de tipo numérico ha sido resuelto en [32] mediante el método de las Características de la teoría de EDPs. En esta tesis se adopta el método de las Características, junto con las siguientes ecuaciones de línea propuestas por Radulet, *et. al.*, [11], para desarrollar un modelo de línea monofásica que incluya efectos Corona y de dependencia frecuencial (o de dispersión lineal).

$$\frac{\partial v}{\partial x} + L_o \frac{\partial i}{\partial t} + \frac{\partial}{\partial t} \int_0^t r'(t - \tau) i(\tau) d\tau = 0 \quad (1a)$$

y

$$\frac{\partial i}{\partial x} + C \frac{\partial v}{\partial t} = 0, \quad (1b)$$

En estas ecuaciones se incluye los efectos frecuenciales mediante el término de convolución de la corriente con la función $r'(t)$ denominada resistencia transitoria. En cuanto al efecto Corona, éste se incorpora expresando al parámetro C de (1b) como una función del voltaje de la línea. La siguiente expresión ha sido propuesta por Gary, *et. al.*, [23]. Debido a que ésta se obtuvo

mediante una gran cantidad de datos experimentales, es la elegida aquí para representar el efecto Corona.

$$C = \begin{cases} C_o & v \leq v_{crit}, \partial v / \partial t > 0 \\ C_o \beta \left(\frac{v}{v_{crit}} \right)^{\beta-1} & v > v_{crit}, \partial v / \partial t > 0 \\ C_o & \partial v / \partial t \leq 0 \end{cases} \quad (2a)$$

En esta expresión v_{crit} representa al voltaje de inyección de Corona cuyo valor se determina mediante la muy conocida fórmula de Peek [23], C_o es la capacitancia geométrica o de línea ideal, r_c representa el radio del conductor en centímetros y β es un parámetro que depende de la polaridad del voltaje. Para una polaridad positiva:

$$\beta = 0.22 r_c + 1.2 \quad (2b)$$

Para obtener $r'(t)$, su imagen en el dominio de Laplace $R'(s)$ es primero relacionada de la siguiente forma con los parámetros convencionales de línea $Z_g(s)$ y $Z_c(s)$, impedancia de tierra e impedancia de conductor, respectivamente:

$$R'(s) = \frac{Z_g(s) + Z_c(s)}{s} \quad (3)$$

Dado que $Z_g(s)$ y $Z_c(s)$ están definidos mediante funciones trascendentales, $R'(s)$ es aproximada aquí mediante una función racional de la siguiente forma:

$$R'(s) = \frac{R_{cd}}{s} + \sum_{l=1}^N \frac{k_l}{s + p_l} + k_\infty \quad (4)$$

donde R_{cd} es el parámetro de resistencia de la línea a frecuencia cero, p_l es el l -ésimo polo de la función, k_l es el l -ésimo residuo de la función en el polo correspondiente y k_∞ es el residuo en $s = \infty$. Posteriormente se obtiene la siguiente expresión para $r'(t)$ al aplicar la transformada inversa de Laplace a (4):

$$r'(t) = R_{cd} u(t) + \sum_{l=1}^N k_l e^{-p_l t} + k_\infty \delta(t) \quad (5)$$

El siguiente paso ahora es incorporar (5) en la ecuación (1a), obteniéndose:

$$\frac{\partial v}{\partial x} + D \frac{\partial i}{\partial t} + R_{cd} i + \vartheta = 0 \quad (6a)$$

donde:

$$D = L_o + k_\infty \quad (6b)$$

y

$$\vartheta = \frac{\partial}{\partial t} \int_0^t \sum_{l=1}^N k_l e^{p_l(t-\tau)} i(\tau) d\tau \quad (6c)$$

Posteriormente, considerando que (6a) y (1b) conforman un sistema hiperbólico de EDPs [9], se les aplica el método de las Características. Se obtiene la siguiente Ecuación Diferencial Ordinaria (EDO):

$$dv + Z_w di + R_{cd} idx + \vartheta dx = 0, \quad (7a)$$

donde:

$$Z_w = \sqrt{L/C} \quad (7b)$$

Esta ecuación es equivalente a (6a) y a (1b), siempre y cuando la propagación en la línea obedezca a la siguiente EDO:

$$\frac{dx}{dt} = + \frac{1}{\sqrt{DC}}. \quad (7c)$$

En forma similar, también se obtiene la siguiente ecuación:

$$dv - Z_w di + R_{cd} idx + \vartheta dx = 0 \quad (7d)$$

equivalente a (6a) y (1b) cuando la propagación en la línea obedece a:

$$\frac{dx}{dt} = - \frac{1}{\sqrt{DC}} \quad (7e)$$

Finalmente, las ecuaciones (7a), (7c), (7d) y (7e) se resuelven numéricamente mediante diferencias centrales. La incorporación en el esquema de solución numérica de ϑ , dado por (6c), se efectúa con el método de la Convolución Recursiva [10]. Tras su discretización, las expresiones (7a), (7c), (7d), (7e), (2a) y (6c) constituyen un modelo digital para la simulación de transitorios en líneas monofásicas incluyendo efectos de dependencia frecuencial y Corona.

El modelo antes descrito se aplica con éxito a varios casos de estudio previamente reportados en la literatura especializada. Quizá el más importante es el de un experimento de campo efectuado por Wagner, et. al., sobre una línea de 2182 m de longitud. La figura 2.4a de la tesis muestra las formas de onda de un impulso registradas en varios puntos a lo largo de la línea. La figura 2.4b muestra las correspondientes formas de onda obtenidas mediante el modelo descrito. De la comparación de estas dos figuras puede verse que las simulaciones que incluyen tanto Corona

como dependencia frecuencial se acercan más a las formas de onda medidas que las simulaciones que solo consideran efecto Corona.

Líneas multiconductoras con efectos de dependencia frecuencial

Para el caso de líneas polifásicas, las ecuaciones (1a) y (1b) pueden generalizarse de la siguiente forma:

$$\frac{\partial \mathbf{v}}{\partial x} + \mathbf{L}_o \frac{\partial \mathbf{i}}{\partial t} + \frac{\partial}{\partial t} \int_0^t \mathbf{r}'(t - \tau) \mathbf{i}(\tau) d\tau = 0 \quad (8a)$$

y

$$\frac{\partial \mathbf{i}}{\partial x} + \mathbf{C}_o \frac{\partial \mathbf{v}}{\partial t} = 0 \quad (8b)$$

donde ahora \mathbf{v} e \mathbf{i} representan los respectivos vectores de voltajes y corrientes en los conductores de la línea, \mathbf{L}_o y \mathbf{C}_o las respectivas matrices de parámetros de inductancias y capacitancias geométricas o de línea ideal y $\mathbf{r}'(t)$ la matriz de impedancias transitorias de la línea. Al igual que para la línea monofásica $\mathbf{R}'(s)$, la imagen en el dominio de Laplace de $\mathbf{r}'(t)$, se relaciona de la siguiente forma con las matrices $\mathbf{Z}_g(s)$ y $\mathbf{Z}_c(s)$, de impedancias de tierra y de conductores, respectivamente.

$$\mathbf{R}'(s) = \frac{1}{s} [\mathbf{Z}_g(s) + \mathbf{Z}_c(s)] \quad (9)$$

Los elementos de esta matriz $\mathbf{R}'(s)$ pueden aproximarse mediante un conjunto de funciones racionales cuyos polos son comunes. Por tanto, la síntesis racional tiene la siguiente forma:

$$\mathbf{R}'(s) \cong \frac{1}{s} \mathbf{R}_{cd} + \mathbf{k}_\infty + \sum_{l=1}^N \frac{1}{s - p_l} \mathbf{k}_l \quad (10)$$

donde \mathbf{R}_{cd} es la matriz diagonal de resistencias en corriente directa de los conductores de la línea, p_l es el l -ésimo polo de las aproximaciones racionales de los elementos de $\mathbf{R}'(s)$, \mathbf{k}_l es la matriz de residuos de $\mathbf{R}'(s)$ en $s = p_l$ y \mathbf{k}_∞ es su residuo en $s = \infty$. La aproximación racional anterior se realiza mediante la técnica denominada Vector Fitting [44]. En el dominio del tiempo, $\mathbf{R}'(s)$ se expresa como:

$$\mathbf{r}'(t) \cong \mathbf{k}_o u(t) + \mathbf{k}_\infty \delta(t) + \sum_{l=1}^N e^{p_l t} \mathbf{k}_l \quad (11)$$

La expresión (11) se incluye en (8a), dando como resultado:

$$\frac{\partial \mathbf{v}}{\partial x} + \mathbf{D} \frac{\partial \mathbf{i}}{\partial t} + \mathbf{k}_o \mathbf{i} + \boldsymbol{\theta} = 0, \quad (12)$$

donde

$$\boldsymbol{\theta} = \frac{\partial}{\partial t} \int_o^l \mathbf{h}(t - \tau) \mathbf{i}(\tau) d\tau.$$

Así pues, las expresiones (8b) y (12) representan el modelo de línea con dependencia frecuencial que aquí se transforma a un nuevo sistema de EDOs mediante el método de las Características.

En el dominio “modal”, estas EDOs incluyen expresiones del tipo:

$$dv_{m,l} + Z_{w,l} di_{m,l} + \gamma_l dt \sum_{q=1}^n \tilde{k}_{o,lq} i_{m,q} + \gamma_l dt \sum_{q=1}^n T_{v,lq}^{-1} \boldsymbol{\theta}_q = 0; \quad l = 1, \dots, n. \quad (13a)$$

y

$$dv_{m,l} - Z_{w,l} di_{m,l} - \gamma_l dt \sum_{q=1}^n \tilde{k}_{o,lq} i_{m,q} - \gamma_l dt \sum_{q=1}^n T_{v,lq}^{-1} \boldsymbol{\theta}_q = 0; \quad l = 1, \dots, n. \quad (13b)$$

Finalmente, las ecuaciones (13a) y (13b) se discretizan mediante diferencias finitas para resolver el problema de propagación de ondas de voltaje y corriente a lo largo de la línea. Las expresiones discretizadas se combinan con el esquema de convolución recursiva para la inclusión de la dependencia frecuencial.

En el caso de líneas excitadas por un campo externo, deben incluirse en (8b) y (12) los respectivos términos:

$$\mathbf{i}_p = -\mathbf{C}_o \frac{\partial}{\partial t} \int_o^h \mathbf{E}_y^{inc} dy \quad (14a)$$

y

$$\mathbf{v}_s = \frac{\partial}{\partial t} \int_o^h \mathbf{B}_z^{inc} dy \quad (14b)$$

El proceso de incorporación de dichos términos a las ecuaciones de propagación es en forma directa.

El modelo con Características y convolución recursiva se valida con tres ejemplos. El primero consiste en una línea excitada por un campo externo, el segundo se refiere a una línea altamente asimétrica y el tercero consiste en un sistema de cables subterráneos. En el primer ejemplo se hace hincapié en la ventaja del método propuesto sobre aquellos basados en ondas viajeras. Adicionalmente los ejemplos dos y tres, que corresponden al caso de líneas homogéneas largas excitadas con fuentes concentradas, arrojan resultados con una precisión muy alta comparados con los de la Transformada Numérica de Laplace.

Modelado de líneas de transmisión no-uniformes para simular transitorios electromagnéticos en el dominio del tiempo

Algunos ejemplos de líneas no-uniformes (LNUs) en sistemas de potencia son: líneas aéreas con catenaria, líneas que cruzan sobre ríos, líneas que entran a subestaciones y estructuras metálicas tales como torres de transmisión. Aquí se adopta una metodología basada en síntesis en el dominio de la frecuencia y convoluciones recursivas para simular transitorios en LNUs. El modelo resultante puede ser aplicado a líneas multiconductoras con dependencia frecuencial.

El modelo propuesto tiene su base en la siguiente ecuación:

$$\begin{bmatrix} v_S \\ i_S \end{bmatrix} = \begin{bmatrix} A & B \\ C & D \end{bmatrix} \begin{bmatrix} v_R \\ i_R \end{bmatrix} = \begin{bmatrix} W_{Fv} & W_{Bv} \\ W_{Fi} & W_{Bi} \end{bmatrix} \begin{bmatrix} \Lambda_F & \\ & \Lambda_B \end{bmatrix} \begin{bmatrix} W_{Fv} & W_{Bv} \\ W_{Fi} & W_{Bi} \end{bmatrix}^{-1} \begin{bmatrix} v_R \\ i_R \end{bmatrix} \quad (15)$$

La expresión (15) representa la relación de las variables voltaje/corriente en los extremos de una línea. La matriz $ABCD$ se calcula a partir de la EDO:

$$\frac{d}{dx} \begin{bmatrix} A(x) & B(x) \\ C(x) & D(x) \end{bmatrix} = \begin{bmatrix} 0 & Z(x) \\ Y(x) & 0 \end{bmatrix} \begin{bmatrix} A(x) & B(x) \\ C(x) & D(x) \end{bmatrix} \quad \begin{bmatrix} A(0) & B(0) \\ C(0) & D(0) \end{bmatrix} = I_{2n \times 2n} \quad (16)$$

Adicionalmente, la expresión (15) describe una transformación de similaridad de la matriz $ABCD$. A partir de lo anterior, se definen las relaciones de voltajes y corrientes en el dominio modal como:

$$\begin{bmatrix} u_{F,S} \\ u_{B,S} \end{bmatrix} = \begin{bmatrix} \Lambda_F & \\ & \Lambda_B \end{bmatrix} \begin{bmatrix} u_{F,R} \\ u_{B,R} \end{bmatrix} \quad (17)$$

Con base a las relaciones (15) y (17), se puede derivar un modelo en términos de ondas viajeras. Dicho modelo está expresado para el extremo receptor como:

$$Y_{C,B} v_R - i_R = T_F \Lambda_B u_{F,S} \quad (18)$$

La correspondiente relación para el extremo emisor se define en forma similar a (18). Cabe mencionar que la propagación en una línea no-uniforme es la misma en las dos direcciones; sin embargo, la admitancia característica vista desde los dos extremos en general es distinta.

A partir del modelo expresado en (18), los parámetros de propagación y admitancias en cada extremo de la línea son sintetizados a través de funciones racionales. Esto permite incorporarlos en realizaciones de espacio-estado. Dichas realizaciones se incorporan en el dominio del tiempo a través de esquemas de convolución recursiva.

El modelo obtenido se aplica en tres casos de LNUs. El primero consiste en una línea simétrica de la cual se tienen resultados experimentales. La simulación con el modelo propuesto reproduce en forma correcta las principales características de las formas de onda experimentales. Aquí se hace la comparación con el método de las Características sin la inclusión de dependencia frecuencial de los parámetros. Para la línea en cuestión se hace notar la diferencia de incluir dicha dependencia. El segundo ejemplo consiste de una estructura vertical. Esta estructura ha sido tomada por varios investigadores para validar sus modelos de LNU. Aquí se compara el modelo propuesto con el de Características. Para este ejemplo de línea, se hace notar que la inclusión de la dependencia frecuencia no es muy importante. Como tercer ejemplo se tiene un caso con características fuertemente no-uniformes. Aquí se tuvieron problemas de oscilaciones los cuales fueron resueltos al aplicar al modelo un esquema de integración distinto (Euler) al utilizado en los otros ejemplos (Regla Trapezoidal).

Conclusiones

En esta tesis se ha reportado el desarrollo de algunas técnicas y modelos para analizar líneas de transmisión. Aunque el enfoque es en líneas de transmisión de energía, se propone que los desarrollos de la tesis podrían ser de utilidad para la solución de problemas de líneas en electrónica y comunicaciones. Se han desarrollado tres modelos de línea.

Para el primero se ha partido de un modelo previamente propuesto en [32] para analizar líneas con efecto Corona, el cual está basado en el método de las Características de la teoría de las EDPs. Este modelo previo ha sido extendido para incluir efectos de variación frecuencial de los parámetros de línea. El modelo extendido ha sido validado a través de resultados experimentales reportados por Wagner y sus coautores [2].

El segundo modelo desarrollado en la tesis permite simular transitorios en líneas polifásicas considerando que los parámetros de línea son funciones de la frecuencia y que la excitación

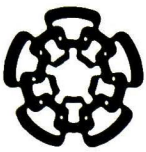
puede ser debida a una fuente distribuida. Dado que este segundo modelo también ha sido basado en el método de las Características, el problema de oscilaciones numéricas no se presenta. Adicionalmente, para el caso de líneas homogéneas largas excitadas con fuentes concentradas arroja resultados con una precisión muy alta.

Finalmente, el tercer modelo presentado en la tesis ha permitido analizar transitorios en líneas no uniformes; es decir aquellas en que, además de la dependencia frecuencial, los parámetros varían con la distancia. Aunque el método de las Características ofrece una base adecuada, aquí se ha utilizado otro enfoque complementario. Éste consiste en primero sintetizar los parámetros de dos puertos de línea en el dominio de la frecuencia y luego aplicar técnicas de ajuste racional y de convolución recursiva para generar un modelo del dominio del tiempo. El modelo resultante ha permitido simular exitosamente casos de líneas que son polifásicas y con parámetros dependientes de la frecuencia y no uniformes. El interés por las líneas no uniformes es nuevo en el ámbito de los sistemas de potencia. Por tanto, todavía no hay criterios para decidir cuando es importante incluir efectos no uniformes en estudios prácticos. Indudablemente, el tercer modelo aquí propuesto facilitará el establecimiento de dichos criterios.

APPENDIX C

List of Publications

1. Abner I. Ramírez, José L. Naredo, Pablo Moreno and Leonardo Guardado, “*Electromagnetic Transients in Overhead Lines Considering Frequency Dependence and Corona Effect via the Method of Characteristics*”, International Journal of Electrical Power and Energy Systems, Elsevier Science LTD, vol. 23/3, pp. 179-188, March 2001.
2. A. I. Ramírez, J. L. Naredo and P. Moreno, “*Method of Characteristics for Transients in Transmission Systems with Frequency Dependent Electrical Parameters*” Submitted to IEEE Trans. on Power Delivery.
3. Abner I. Ramírez, Adam Semlyen and Reza Iravani, “*Modeling Non-Uniform Transmission Lines for Time Domain Simulation of Electromagnetic Transients*”. Submitted to IEEE Trans. on Power Delivery.



**CENTRO DE INVESTIGACION Y DE ESTUDIOS AVANZADOS DEL IPN
UNIDAD GUADALAJARA**

El Jurado designado por el Departamento de Ingeniería Eléctrica del Centro de Investigación y de Estudios Avanzados del Instituto Politécnico Nacional, Unidad Guadalajara, aprobó la tesis: **Modelos avanzados para la Simulación de Transitorios Electromagnéticos en Líneas de Transmisión** del C. Amner Israel Ramírez Vázquez, el Día 5 de Octubre de 2001.

Dr. José Luis Naredo Villagrán
Investigador Cinvestav 3B
CINVESTAV del IPN
Guadalajara

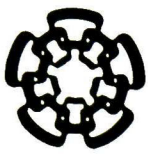
Dr. Alexander Loukianov
Investigador Cinvestav 3 A
CINVESTAV del IPN
Guadalajara

Dr. Pablo Moreno Villalobos
Investigador Cinvestav 3 A
CINVESTAV del IPN
Guadalajara

Dr. Juan Manuel Ramírez Arredondo
Investigador Cinvestav 3 A
CINVESTAV del IPN
Guadalajara

Dr. Meza Reza Iravani
Profesor Investigador
University of Toronto
Toronto, Ontario, Canadá

Dr. Francisco de León Gómez Maqueo
Profesor Investigador Titular C
Universidad Michoacana
Morelia Michoacán



**CENTRO DE INVESTIGACION Y DE ESTUDIOS AVANZADOS DEL IPN
UNIDAD GUADALAJARA**

El Jurado designado por el Departamento de Ingeniería Eléctrica del Centro de Investigación y de Estudios Avanzados del Instituto Politécnico Nacional Unidad Guadalajara, aprobó la tesis: “**Advanced Models for Electromagnetic Transient Simulation of Power Transmission Lines**” del C. Amner Israel Ramírez Vázquez, el día 5 de Octubre del 2001

Dr. José Luis Naredo Villagrán
Investigador Cinvestav 3B
CINVESTAV del IPN
Guadalajara

Dr. Alexander Loukianov
Investigador Cinvestav 3A
CINVESTAV del IPN
Guadalajara

Dr. Pablo Moreno Villalobos
Investigador Cinvestav 3A
CINVESTAV del IPN
Guadalajara

Dr. Juan Manuel Ramírez Arredondo
Investigador Cinvestav 3A
CINVESTAV del IPN
Guadalajara

Dr. Meza Reza Irvani
Full-professor
University of Toronto
Toronto, Ontario, Canada

Dr. Francisco de León Gómez Maqueo
Profesor Investigador Titular C
Universidad Michoacana
Morelia, Michoacán



CINVESTAV
BIBLIOTECA CENTRAL



SSIT000003917